Supplementary proposal for the repair of the Super–Kamiokande detector

February 1, 2002 – January 31, 2003

Submitted on behalf of the U.S. Super–Kamiokande Collaboration by:

Principal Investigator – Henry W. Sobel
Professor of Physics
University of California, Irvine

Prepared for the U.S. Department of Energy, Division of Physical Research, under GRANT DE–FG03–91ER40679.

Contents

List of Figures

1 Introduction

On November 12, 2001, the Super–Kamiokande tank was within 7 meters of being refilled following the summer's refurbishment work. Just after 11 a.m., Japan Standard Time, the physicists on shift in the mine felt a strong rumbling motion, similar to an earthquake. Subsequent investigation revealed extensive damage to both the inner and outer detectors. The University of Tokyo appointed a committee to investigate the incident. Its charge was to tabulate the damage, establish the mechanism which led to the destruction, and ensure that it cannot recur when the detector is repaired and resumes operation.

It is our intention to repair the detector and return it to operation as soon as possible. Unfortunately, Hamamatsu Corporation will require about four years to manufacture the seven thousand 20-inch inner detector replacement phototubes needed. Thus, it is impossible to restore the inner detector to full photocathode coverage in time to restart the K2K experiment. We plan, therefore, to redistribute the remaining undamaged 20-inch tubes, augmented with spares on hand, to uniformly populate the inner detector at one half the original density. The K2K experiment, and most other aspects of our experimental program, can continue effectively in this configuration while replacement tubes for the inner detector are manufactured. Fortunately, it is possible to obtain the much smaller number of 8-inch tubes necessary on a shorter timescale; we are proposing to restore the outer detector to full sensitivity immediately.

This proposal describes the maintenance work which preceded the November 12 incident, summarizes the information presented to the University of Tokyo committee, explains our plan to return the detector to operation (including measures to prevent future damage), outlines the expected performance of the detector and its physics program during the interim period with reduced photocathode coverage, and briefly discusses the future JHF long-baseline program, which will rely on Super–Kamiokande as a far detector.

2 Summary of Summer 2001 Maintenance

After several years of planning and preparation, the replacement of malfunctioning PMT's in the Super–Kamiokande detector commenced in July 2001. This was the primary effort of the maintenance shutdown. The U.S. groups' responsibilities for the detector upgrade involved mainly the outer detector (OD). Data-taking ceased on July 16, when the process of draining the tank began. This date was dictated by the end of the beam cycle at KEK.

2.1 Outer Detector

A total of 280 8-inch Hamamatsu PMT's were purchased for the upgrade. These tubes used the proven base potting technique developed for the 50-cm inner detector PMT's. Minor modifications were made in the design to accommodate our polyethylene cable jackets. The design of the new tubes' base chain was

centered on preserving the shape of the PMT output pulse in spite of the faster timing characteristics of the new tubes. While still somewhat faster than the old tubes (purchased in 1985 for IMB), the QTC electronics seems to work fine with the new tubes. Their two-month exposure to water prior to the 12 November incident suggests the design of the base potting was satisfactory.

It was decided early in the upgrade planning not to open the cable baffles between the detector and the electronic huts. The design of the baffles and safety considerations dictated this decision. As a consequence, the new PMT's had to be spliced to the existing cables. Considerable design work and testing were devoted to development of a waterproof splice that could be easily made in the field from boats and/or from the top and bottom framework of the detector. The final design employed SHV connectors that are sealed with heat-shrink tubing and tape. A number of splices were tested in water at 85 psi for 5 or more weeks without any failures. Results from the two-month exposure of the splices to water prior to the November 12 incident suggest a successful design.

A total of 272 tubes (of 1885) were replaced. Approximately 130 or nearly half of the failures had occurred in the first year of detector operation. Since then, the failure rate had been fairly constant at approximately 3 tubes per month. The main failure mode of the tubes was identified during the upgrade activities as water seepage into the cables that ultimately provided a low resistance path between the high-voltage and the cable ground shield, shorting out the power supply to the tube. Thirteen of the failed tubes were not replaced and another 15 failed shortly after splicing. The 13 had cables that were obviously waterlogged and the other 15 are assumed to have the same problem. (These 15 were done early in the replacement process when the workers were less experience in recognizing the water problem. The use of boats as the tank drained prevented the revisiting of these tubes.) As noted above, the main failure mode appears to be water seepage into the cables. The IMB housings functioned well. Only about 10% of the housings of the failed tubes show signs of water; in the rest, the desiccant shows no sign of moisture. A smaller percentage of the tubes had real base problems, had lost their vacuums, or had failed for unknown reasons.

2.2 Other U.S. Upgrade Tasks

In addition to the photomultiplier replacement, several other important improvements to the experiment were performed in conjunction with the upgrade:

- The High Voltage Distribution and Signal Pick-off Boards (paddle cards) were redesigned and installed over the three month period from November 2000 to January 2001. The new cards are considerably more robust than their predecessors and have features dictated by the experiences gained in 5 years of detector operation. The key design change was the incorporation of a front panel switching system to control the application of high voltage to the individual PMT's. Since each HV channel serves 12 PMT's, easy control and isolation of the voltage to each PMT is necessary for the

maintenance of the OD. Diagnosis and correction of PMT problems are greatly facilitated by the new system, which has already proven its worth. The new cards also provide a more secure coupling of the PMT output signal to the QTC cards, a previous source of lost data associated with system maintenance.

- A highly successful DT generator for detector calibration was designed and constructed by the U.S. groups. A paper was published detailing the design and operation of the DT generator.

- Hardware and software were developed which allowed the detector threshold to be lowered to 4.5 MeV. This U.S.-led effort greatly enhanced the solar neutrino physics capabilities of the detector.

2.3 Inner Detector

A total of 233 inner detector (ID) PMT's were replaced. The work proceeded in parallel with the OD work described above. As for the OD, each failed tube's cable was cut and the replacement tubes short cable stub was spliced onto it. The splicing technique was similar to that used in the OD work. The ID work was complicated by the large size of the ID tubes. Replacement of the top and bottom tubes required access to tubes from both the ID and the OD. This involved removing some of the top OD tubes and also extensive cutting and patching of the opaque Tyvek used to isolate the two regions of the detector. The top and wall work was done using a Styrofoam floating floor system and small boats. The floating floor allowed the work crews to safely handle the large and heavy tubes and tube modules. Retired Kamioka miners, closely supervised by physicists, performed much of this work. The top and wall work involved the replacement of 28 and 143 tubes, respectively.

Replacement of the 62 dead tubes in the bottom layer of the ID presented a number of special problems. Given that the tubes needed to be out of the water, boats and a floating floor could not be employed. One possibility, working from the OD below, was considered, but rejected. This option would have involved disassembly of many OD supermodules to gain the needed access. In addition, access from above would have still been needed to permit lowering the tubes into the OD. Instead, an alternative scheme was developed. Large, thick Styrofoam mats were placed across the surface of the tubes to act as a working platform (see Figure 1). These mats distributed the load of workers over many PMT's, so that the tubes' collective structural strength would be adequate to support them. (A third possible procedure, involving a working surface supported by the structure to which the tubes themselves were affixed was deemed impractical since it would have required long, spindly support legs and been very difficult to deploy.) A full-scale mock-up of the mat-on-tube support system was built at ICRR in Tokyo and many tests were performed with no apparent damage to the tubes involved. This and other tests in which tubes were actually broken with heavy weights seemed to prove that the proposed system was safe and effective.

Figure 1: The technique used to replace phototubes on the bottom of the inner detector.

3 The November 12 Incident

3.1 Inner Detector Damage

A series of implosions destroyed 6,777 20-inch photomultipliers of the inner detector's original complement of 11,146. In addition, the plastic sheeting used for optical isolation between the inner and outer detectors was destroyed. There was no damage to the electronics or the high voltage system.

3.2 Outer Detector Damage

The outer detector, a responsibility of the U.S. groups, lost about 1,160 8-inch photomultipliers (out of 1885) and much of the opaque/reflective Tyvek barrier that separated it from the ID. Also lost were an estimated 600 waveshifter plates used to enhance the light collection area. The estimated number of waveshifter plates damaged is based on a scan of a small portion of the detector with an underwater robot camera. The exact number will be tabulated when the detector is completely drained in March 2002. Damage to these plates consists mainly of large cracks through the mounting holes and/or large sections broken from the plates. There was some very minimal damage to the high voltage system.

3.3 Water Tank Damage

Although a full inspection of the tank structure has not yet been possible, there does not appear to be any damage. There is, however, a small water leak. Microphones deployed within the detector have isolated the leak to one of three areas on the bottom of the tank. This will be investigated and repaired when the tank is emptied.

3.4 Onset

Although the tank was only partially filled, the detector was fully operational and taking data on "Supernova Watch" at the time of the first implosion. Thus, the onset of the damage is documented; after 30 msec, the data volume exceeded the throughput capacity of the data acquisition system and no further information is available. These data localize the first tube to implode within a fairly small region in a corner of the inner detector's bottom plane (see, for example, Figure 2). Data runs recorded from the time refilling began were also scrutinized, since the tube we are searching for likely showed early indications of a problem by flashing or noise. We believe we can narrow the possibilities to two adjacent bottom tubes. One of these was newly installed during the maintenance period, and the other was installed during the initial detector construction in 1996.

3.5 Destruction Mechanism

Data recorded in the first 30 msec made clear that the incident was precipitated by implosion of a single 20-inch tube which initiated a pressure wave, causing the failure of adjacent tubes and subsequently propagating throughout the detector in a chain reaction which eventually ended a few meters below the water's surface. To test this hypothesis and better understand the mechanism, numerical and *in situ* simulations were performed.

3.5.1 Numerical simulation

Hydrodynamic simulations were carried out approximating the shape of the photomultiplier tubes. These simulations indicated that a shock wave pulse reaches adjacent PMT's roughly 10 msec after an implosion (see Figure 3), with an amplitude of about 100 atm (the precise value depends on the details of the simulation). The pulse width, however, is very short, some 10's of microseconds, thus raising the question of whether the shock would be sufficient to destroy an adjacent tube. This question could only be addressed experimentally.

3.5.2 Experimental simulation

Since the detector was still almost full of water, the implosion pressure pulse was studied *in situ*. An array of nine 20-inch tubes, separated by the standard spacing of 0.7 meters, was lowered to a depth of 30 meters (see Figure 5). A pneumatic firing pin broke the center tube of the array, while pressure sensors and strain gauges mounted on the surrounding tubes recorded the time profile of the resulting pressure pulses. In Figure 4 a sample of the pressure, strain and acceleration data recorded for each test is shown. A high-speed camera was also employed to record the tests. Figure 6 shows details of the pressure pulses arriving at each PMT and the order of their destruction. The resulting data were compared to the simulations. The procedure was repeated three times and in all cases the surrounding tubes were destroyed by pressure pulses similar

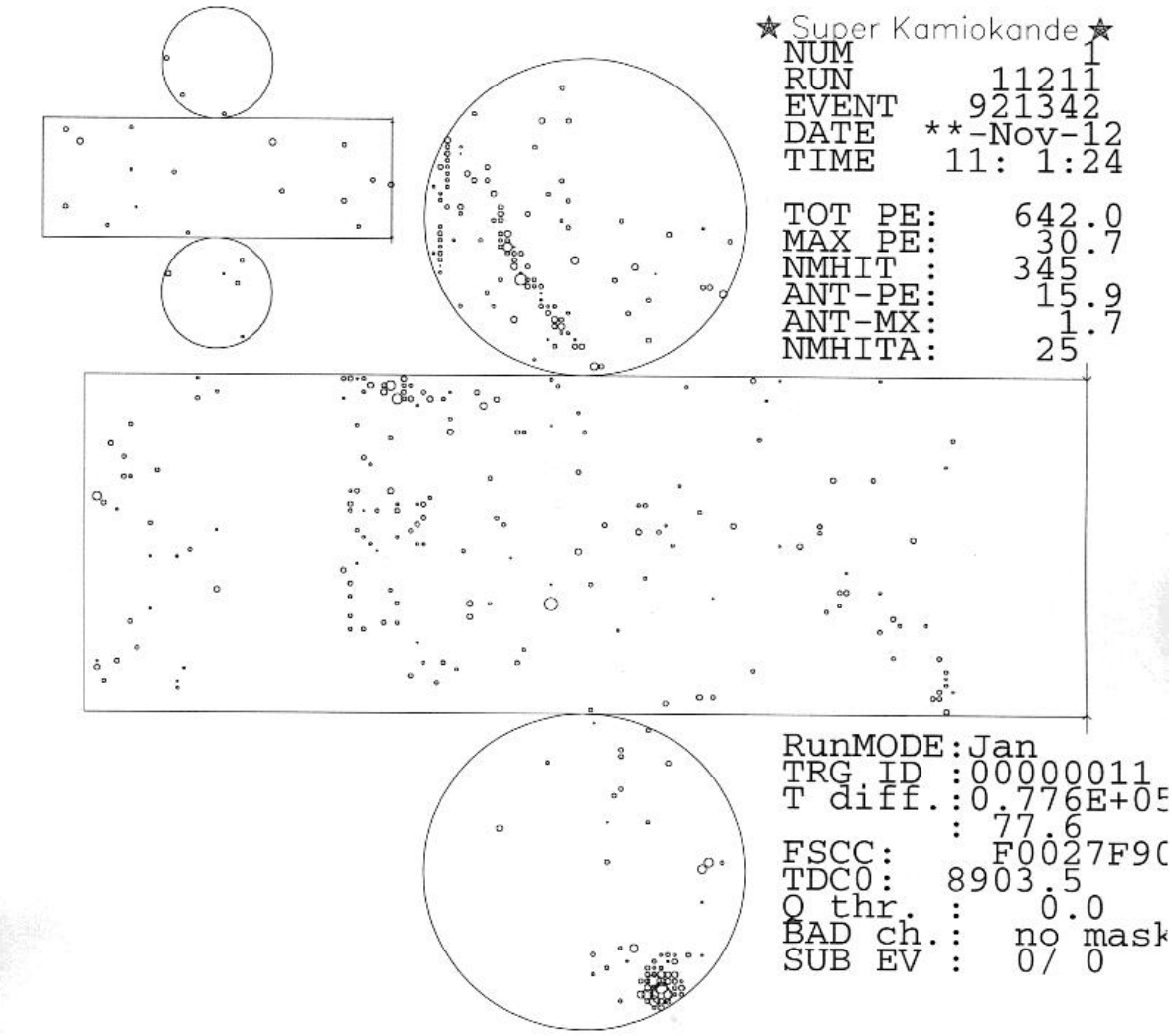

Figure 2: One of the event displays recorded during the beginning stages of the incident. A cluster of tubes with a large amount of light is seen on the bottom of the detector. One of two tubes in this region is believed to be the initial failure.

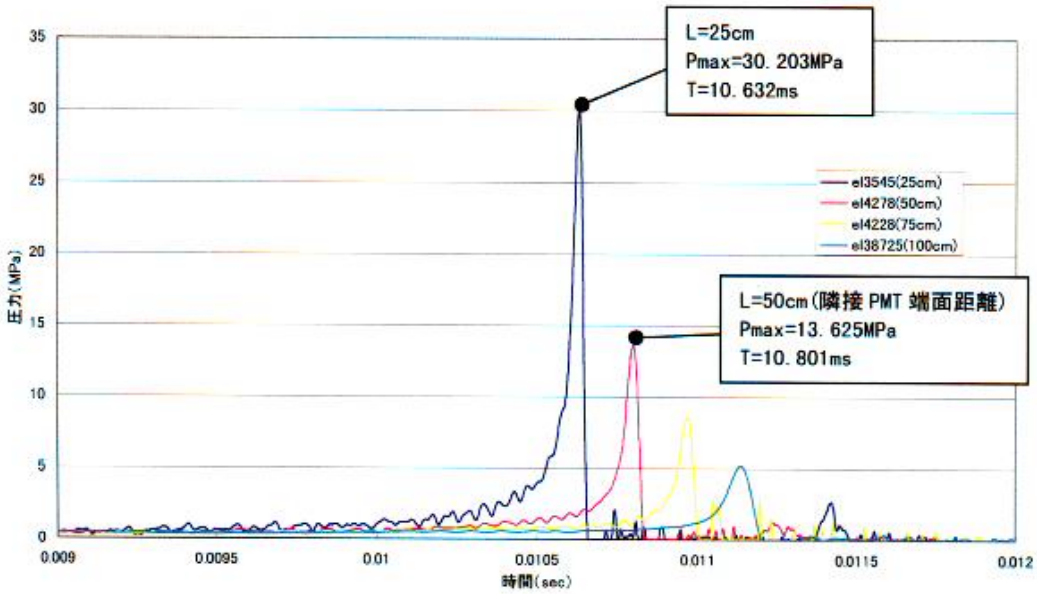

図-3　圧力時刻歴

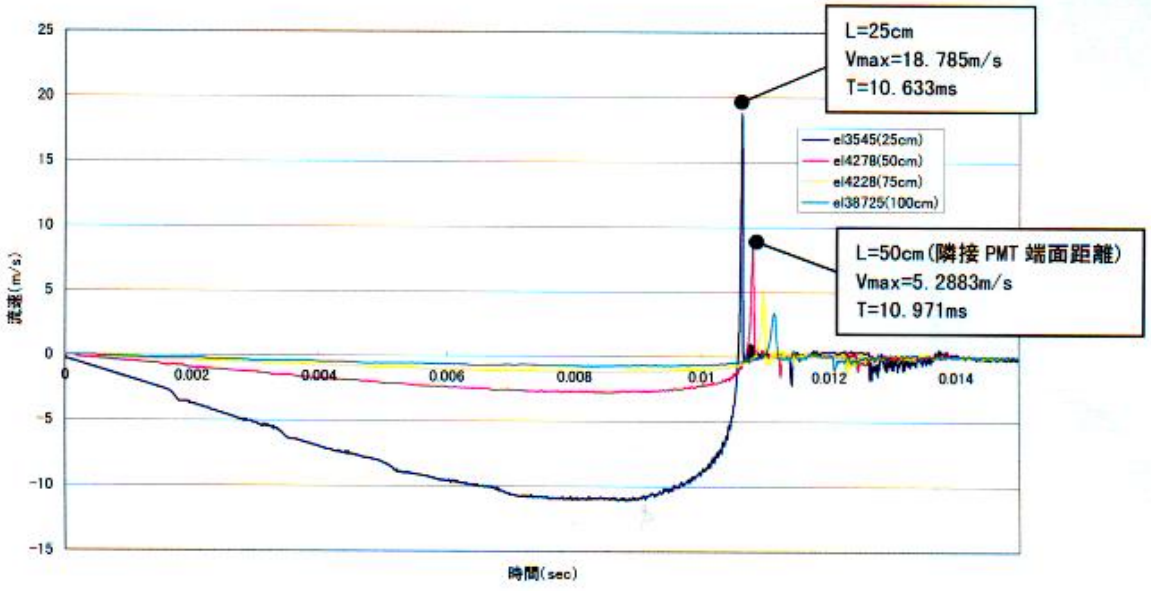

図-4　流速時刻歴

Figure 3: Results of a hydrodynamic simulation. Top figure: The amplitude and timing of pressure pulses expected at nearby locations after a PMT implosion. In Super-K the 20-inch tubes are separated by 0.7 meters. Bottom figure: The water velocity and timing expected at nearby locations after a PMT implosion.

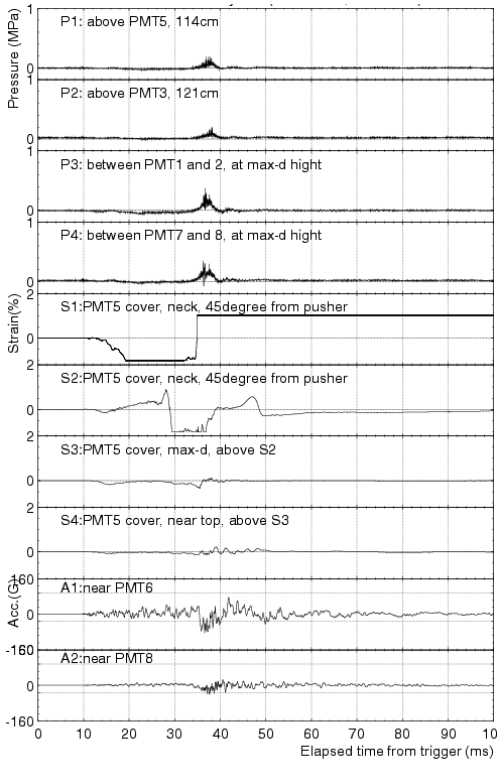

Figure 4: Sample data recorded for each test. Pressure, strain and acceleration are recorded at various points surrounding the center tube.

to those predicted by the simulation, thus proving that the failure of a single 20-inch tube can initiate a chain of collapses.

The simulation predicts that the pressure of the shock wave is proportional to (external pressure)$^{1.9}$ (see Figure 7); thus the survival of PMT's near the surface of the detector can be explained. To confirm this prediction, we performed implosion experiments at 10 and 3 m depths. In all cases, none of the surrounding tubes were broken. Data from the pressure sensors agreed with the predictions of the simulation within experimental errors.

3.6 Cause of the First Implosion

Since implosion destroys the glass envelope of a PMT completely, and the remains of the first tube are mingled with thousands of others, we can never establish the reason it failed with complete certainty. Even so, we investigated the history of the two suspected tubes as well as the properties of 200 others removed during the maintenance period. The recently removed tubes were of particular interest since it was possible that the long immersion of PMT's in the

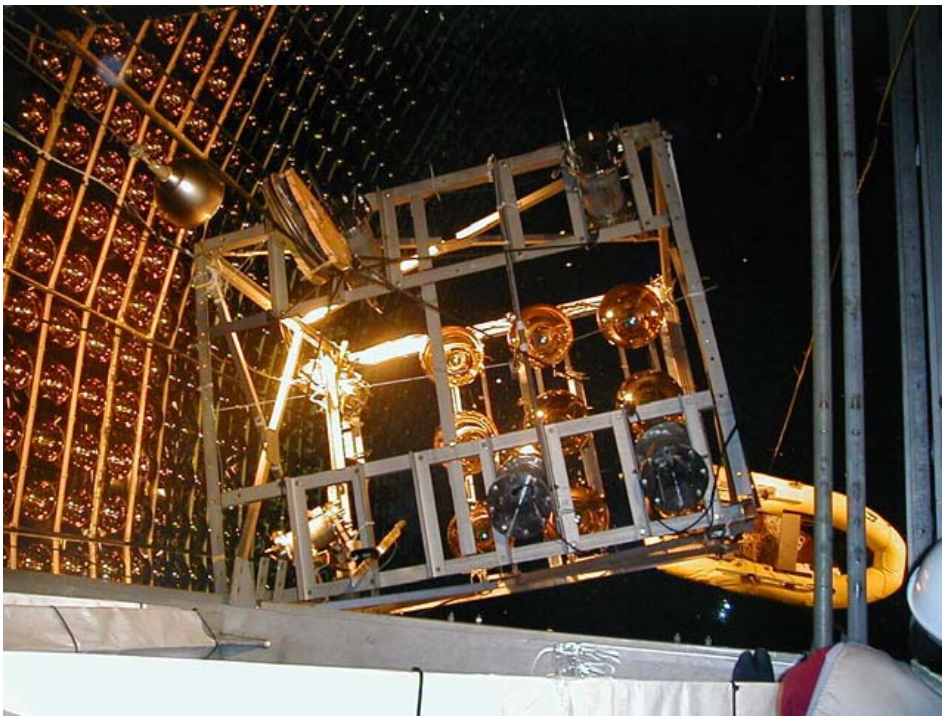

Figure 5: Lowering a frame of nine tubes into the detector for implosion tests.

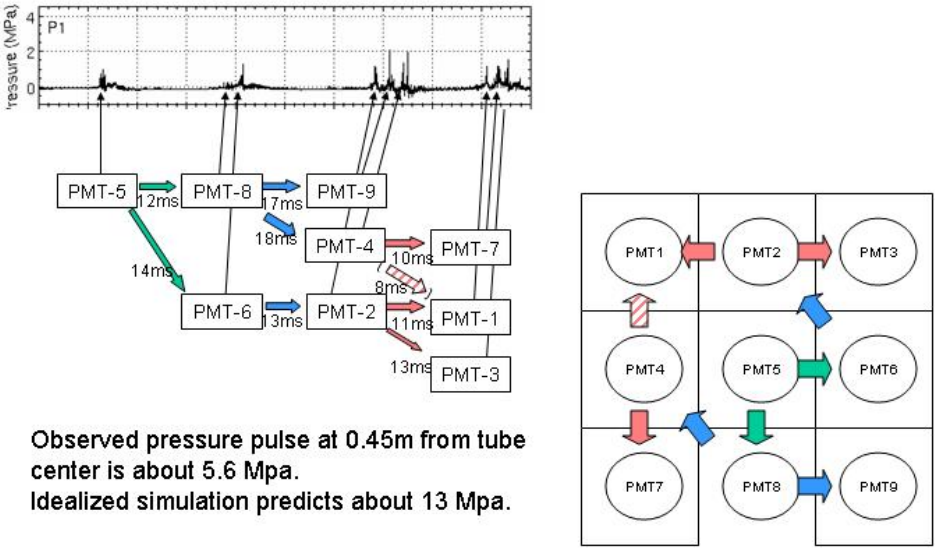

Figure 6: The data from one of three implosion tests performed with unprotected tubes.

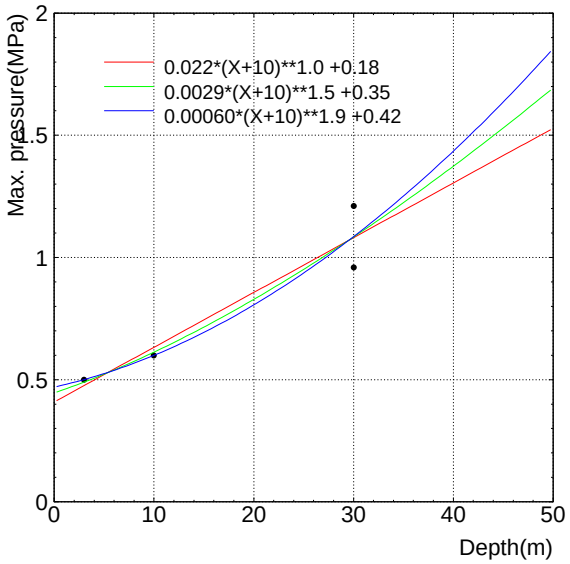

Figure 7: Predicted pressure vs. depth (three simulations with slightly different assumptions) compared with measured data (points).

highly purified detector water might have compromised their glass envelopes' structural properties. A variety of tests were performed, including: chemical composition of the glass, strength, crystallization, temperature cycling, pressure cycling, glass thickness, etc. All of the parameters tested were within the required limits and none appeared to have changed during five years underwater.

Our suspicions were thus redirected towards the installation procedure used for replacement of the bottom tubes. During this process, we constructed a foam floor which rested on the faces of the bottom tubes. As senn in Figure 1, technicians walked on this floor to access the tubes. Although extensive tests indicated the procedure was safe before it was adopted, we have now tested it again with about eight times the normal load. One of the tubes tested cracked under these conditions. We thus believe that the bottom tube replacement procedure could have caused the initial implosion by slightly cracking a tube.

In addition, each of the 200 PMT's removed during the maintenance was carefully inspected visually. In one tube, evidence of damage from impact was found at the neck. This PMT malfunctioned soon after initial installation in 1996, while it was OK before the installation. Since we have now documented evidence for physical damage to a tube during installation, we cannot exclude the possibility that one of the newly installed tubes was also damaged in this way.

Thus, these two possibilities remain as possible causes of the incident. In either case, a hairline crack in a damaged PMT would have caused it to fail catastrophically if the gradually increasing water pressure at the bottom of the tank exceeded the glass envelope's reduced structural tolerance during refilling.

4 Analysis and Remedial Measures

Although a flawed maintenance procedure, or careless installation of a particular tube, may have been the proximate cause of the catastrophic damage to the detector, failure to anticipate and forestall the chain reaction failure mode must be considered the true culprit. In an experiment employing some 13,000 PMT's and designed to run for a decade or more, it is implausible to assume that no tube will ever break, for whatever reason. Nor would elaborate precautions to preclude the possibility of individual tube failures (for instance, by enclosing each in a pressure-tight housing) be cost-effective, given the highly redundant nature of the PMT array and considering that any single tube is, ultimately, expendable. Instead, we must accept that tube failures, although evidently rare, may occur from time to time and prevent failure of a single PMT from damaging others nearby.

4.1 Pressure-damping Enclosures

To prevent recurrence of the chain reaction, we have designed individual enclosures for the 20-inch tubes whose purpose is to spread out the energy released by an implosion over a longer period of time. In this way, the amplitude of

Table 1: Tube enclosure configurations

Configuration	Thickness	Date	Depth	Notes
Acrylic I	Acrylic 6mm	Jan.22	27.3m	0.35% hole fraction
Acrylic II	Acrylic 6mm	Jan.24	27.1m	.90% hole fraction
FRP I	Fiberglass 3mm + acrylic 6mm	Jan.23	27.2m	0.45% hole fraction
FRP II	Fiberglass 7mm + acrylic 15mm	Jan.25	27.0m	$\leq$0.01% hole fraction
FRP III	Fiberglass 5mm + acrylic 15mm	Jan.26	26.9m	$\leq$0.01% hole fraction
FRP IV	Fiberglass 5mm + acrylic 10mm	Jan.26	26.9m	$\leq$0.01% hole fraction
FRP V	Fiberglass 3mm + acrylic 15mm	Jan.27	26.8m	0.20% hole fraction
FRP VI	Fiberglass 5mm + acrylic 15mm	Jan.27	26.7m	0.20% hole fraction
SUS I	Stainless 1mm + acrylic 10mm	Jan.23	27.1m	0.5% hole fraction
SUS II	Stainless 2mm + acrylic 10mm	Jan.25	27.0m	0.5% hole fraction
SUS III	Stainless 6mm no front cover	Jan.26	26.9m	0.5% hole fraction

the pressure pulse is damped to a level which will not damage nearby tubes. A number of prototypes were constructed (see Table 1) and tested at depth using the familiar nine-tube arrays. The fiberglass versions consist of a formed fiberglass sleeve covering the bottom and neck of the tube, flanged to an acrylic dome covering the photocathode. Each of the containers is perforated with holes allowing water to fill the region between the tube and the inside of the container. The size and number of the holes are chosen to slow the water flow into the container when a tube breaks.

The container need not be very strong, since it is only exposed to a high pressure when a PMT implodes. Finite element stress calculations were done to evaluate the pressure on various points of the containers (see Figure 10). Based on these tests and calculations, the container's required thickness is either 15mm acrylic + 5mm fiberglass, or 10–15 mm all-acrylic. Pictures of these two configurations are shown in Figure 8 and Figure 9. We estimate a $\sim$10% loss in light collection due to the 15mm thick acrylic case.

The amplitude of the pressure wave generated by a tube in its protective case is reduced by over a factor of one hundred from that of an unprotected tube. When outfitted with these enclosures, the failure of the center tube in an array of nine does not damage the surrounding tubes. This is true *even when the surrounding tubes are not themselves protected by enclosures.* Since we intend to enclose all tubes, and since the energy released decreases with depth the test provides a conservative demonstration of the robust nature of the protection mechanism.

4.2 Failure Scenarios

One must also reckon with the possibility that an outer detector tube might fail and cause a chain reaction, by destroying a nearby inner or outer detector tube. The energy released when a photomultiplier tube implodes is proportional to its volume, therefore, at a given depth, the energy released when an outer

Figure 8: An all-acrylic tube enclosure design.

Figure 9: A fiberglass and acrylic tube enclosure design.

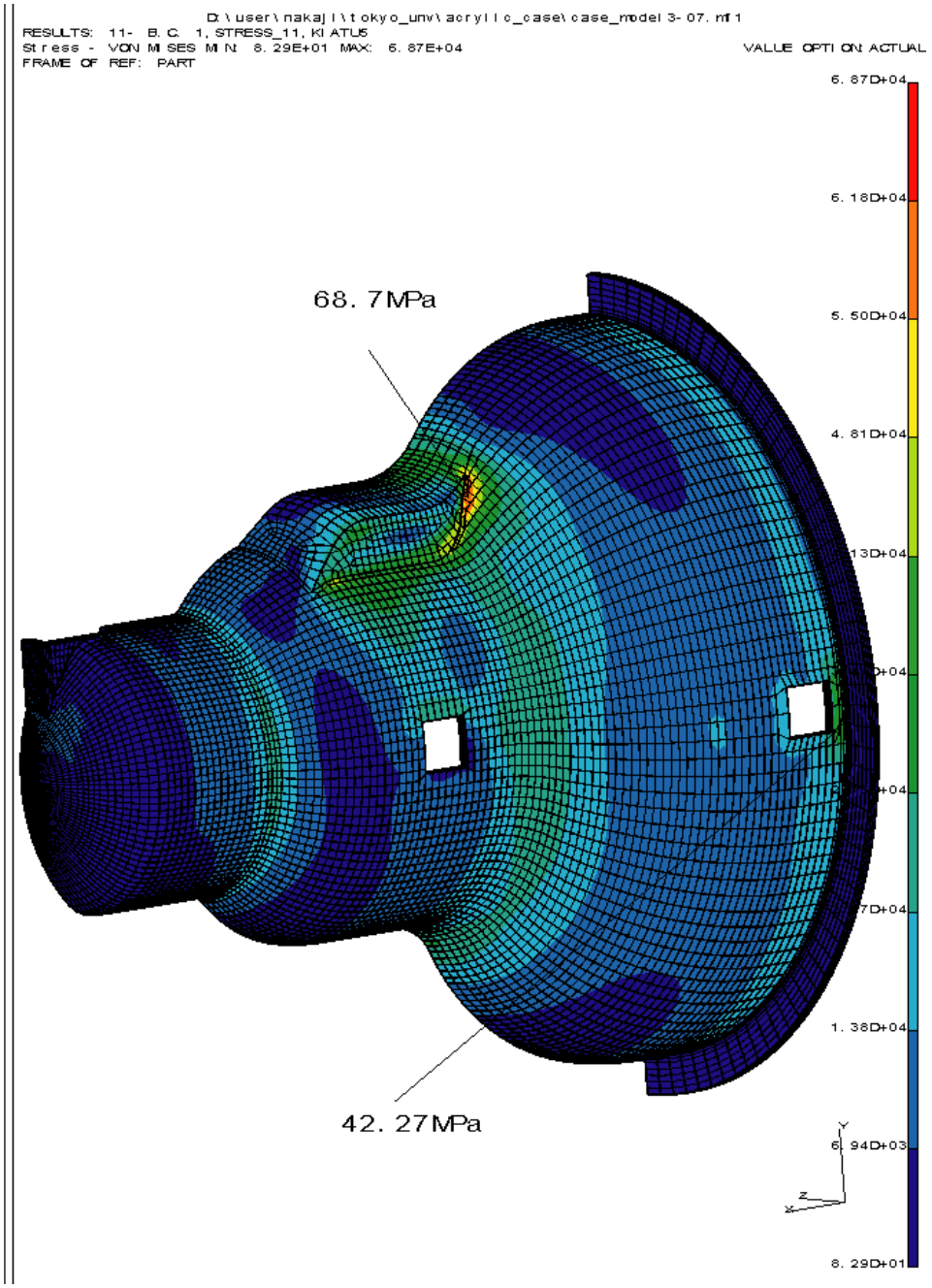

Figure 10: Finite element stress calculation on fiberglass portion of the tube enclosure design.

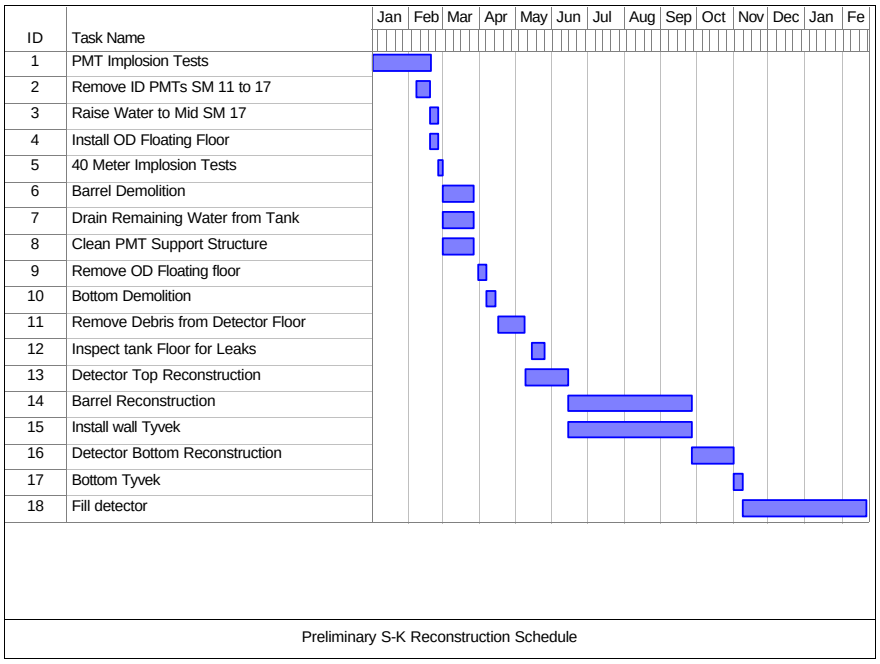

Figure 11: The reconstruction schedule with emphasis on outer detector work.

detector phototube fails is about a factor 15 less than for an inner tube. This difference, combined with the much larger outer detector tube spacing, prevents outer tubes from initiating a chain reaction of other outer detector implosions. Thus, if, in spite of its protective housing, an inner tube implosion somehow destroys a nearby outer tube, the incident would remain localized. If an outer tube fails and, in spite of the greatly reduced energy release, destroys a nearby inner tube, once again, the protective case would localize the incident. In fact, during the recent maintenance period, we found several outer detector tubes near the bottom that had broken without harmful effects on their neighbors, demonstrating that implosion of an 8-inch tube does not harm nearby 20-inch tubes, and that outer detector chain reactions do not result from these failures.

5 Repair and Recommissioning Schedule

Figure 11 shows a preliminary reconstruction schedule with emphasis on the outer detector (OD) work and includes inner detector (ID) work only as it impacts the OD effort.

Removal of the broken tubes and the damaged waveshifter plates and Tyvek

will be the first step in the reconstruction process. This operation will begin in late February. Mitsui, the main Japanese contractor for the detector vessel and PMT support structure, will construct a floating floor that will completely circle the OD. From this floor, we will strip the detector of its opaque Tyvek, remove the damaged waveshifter plates and cut out the damaged tubes. The contaminated outer wall Tyvek will also be removed at this time. This is further required by the need to scan the walls for leaks. During the process, the serviceable tubes and waveshifter plates as well as the entire PMT support structure and detector tank walls will be washed to remove the residue from the water contaminated by photocathode material as well as other remains from the accident. The operation will progress as draining the detector tank lowers the floating floor. When the demolition operation reaches the level where glass shards and other materials makes the work hazardous, the main effort will be taken over by Mitsui workers with the guidance of physicists. As shown in Figure 11, this process is estimated to require about 3 weeks.

The bottom PMT layer of the detector will be similarly stripped. Following this the glass and other rubble on the detector floor will be removed, as will the floor Tyvek. The detector floor will then be scanned for leaks. The present schedule calls for this process to be completed by mid-May.

Reconstruction of the detector will proceed in 3 phases, top, wall, and bottom:

- The top reconstruction for the OD is not driven by the replacement of OD tubes. Only 8 have failed, of "natural" causes unrelated to the 12 November incident. However, all of the ID tubes will be removed and distributed, at half density, in the deeper portions of the detector. Tubes that were only a few meters below the water level at the time of the accident, and which survived will replace them. (These tubes will be inspected for damage and pressure tested before re-installation.) This removal and replacement operation will require that the top OD Tyvek be completely stripped and that all OD tubes be temporarily removed. The top operation will take approximately 1 month.

- The barrel reconstruction involves the replacement of about 840 OD tubes. This work will be done from gondolas and will take about 90 days. As was discovered during last year's upgrade, water seepage into the signal/HV cable was the main source of failure of the OD tubes. This is a potential problem for the reconstruction as it is anticipated that the imploded tubes will have their cables exposed to the water. To mitigate against this problem we will splice all cables at a shallow depth near the top of the detector so as to provide a long cable path between the splice and the water-immersed cable end. Typically this distance will exceed 20 meters and should provide an effective water barrier.

- The bottom reconstruction involves the replacement of all 308 8-inch PMT's. Once again all Tyvek will be replaced as the ID tubes will be installed from the OD. Our small statistics sampling suggests that the

bottom waveshifter plates largely survived the November 12 incident. The bottom operation will take approximately 5 weeks.

The budget includes costs for travel, housing, and living expenses for the physicists and technicians involved in the repairs.

6 Detector Performance

6.1 Inner Detector

Detailed Monte Carlo studies of detector performance with reduced photocathode coverage are both labor- and CPU-intensive, and will require considerable revision and re-tuning of the reconstruction tools; in the past months, these studies have necessarily taken second priority to investigation and mitigation of the damage to the detector itself. For the present, we rely on a combination of preliminary studies specific to the reduced-coverage Super–Kamiokande detector and extrapolations from the known performance of the full Super–Kamiokande, Kamiokande II and 1-kton (K2K) detectors.

The obvious point of reference for the performance of a water Cherenkov detector with 20% photocathode coverage is the Kamiokande II experiment, which was instrumented to the identical specification.[1] Such comparisons are useful, but not without limitations, since Kamiokande II was much smaller than Super–Kamiokande. While the slightly increased light attenuation for events in the center of Super–Kamiokande may adversely affect the lowest energy processes, more important are geometrical issues of scale. Since 20-inch phototubes are employed in all cases, for a given level of photocathode coverage, each tube in a smaller detector will subtend a larger fraction of the solid angle from a point inside the fiducial volume of a smaller detector. Equivalently, one can say that the projection of neighboring Cherenkov cones onto the PMT plane will be more spatially separated (i.e. will tend to overlap less) in a larger detector. The magnitude of this effect can be estimated from Monte Carlo studies of the Super–Kamiokande and 1-kton detectors with equal 40% photocathode coverage but disparate sizes. For most quantities of interest, the performance of the 1-kton detector is somewhat inferior to that of Super–Kamiokande, despite equal photocathode coverage. Similarly, due not only to geometry but also to improvements in the reconstruction tools and photomultiplier time jitter during the intervening ten years, we believe the performance of Kamiokande II represents, in almost every instance, a very pessimistic *lower bound* on the performance of Super–Kamiokande with 20% photocathode coverage.

[1] Note that the estimated 10% loss of light collection per PMT due to the pressure-damping enclosures is comparable to a 7% loss in Kamiokande from the μ-metal mesh which shielded each PMT from the geomagnetic field. In Super–Kamiokande the geomagnetic field is nulled over the entire detector volume by a compensating coil around the tank.

6.1.1 Trigger threshold

The hardware trigger threshold is relatively unimportant in determining the low-energy capabilities of the detector. Thanks to the Intelligent Trigger system developed and maintained by the U.S. groups, the true "threshold" for physics analyses is determined not by the hardware, but by the ability to reconstruct event vertices and directions; with acceptable vertex and directional resolution, interactions in the fiducial volume can be separated from entering background and (for solar neutrinos) correlated with the Sun. This is a major advantage of Super–Kamiokande with respect to the earlier Kamiokande II experiment. As the next section demonstrates, Super–Kamiokande will still be able to measure ^{8}B neutrinos above 6–7 MeV (electron energy) if the inner detector is restored to half the original photosensor coverage.

The analysis threshold is ultimately determined by the signal efficiency and remaining background level. It is difficult to determine the analysis threshold exactly since the photomultipliers themselves are believed to be a significant source of low-energy background, although precisely what fraction is uncertain. Thus there will be some competition between the loss of light collection, which will drive the threshold up, and the absence of half the PMT's (and their associated background), which may compensate to some extent by reducing the background. The net effect of this competition will only be clear after the detector is recommissioned.

6.1.2 Vertex resolution

For both low-energy and high-energy analyses, vertex resolution is essential for defining the fiducial volume and facilitating accurate measurement of event properties (energy, particle identification, etc.).

Figure 12 shows that 80% of the solar neutrino events reconstructed between 5 and 5.5 MeV have a fit vertex not farther than 4 meters (which is sufficient to reconstruct energy and direction) from the true interaction vertex. While reconstruction efficiency of 5 MeV electrons is rather low (about 50%), an analysis threshold of $6-7$ MeV can be reached with good efficiency (80% to 90%).

The estimated vertex resolution for fully-contained, single-ring, sub-GeV events is 30 cm with 40% Super–Kamiokande photocathode coverage; in Kamiokande II, the corresponding vertex resolution was 60 cm. This difference is due, in large measure, to improvements in the 20-inch phototubes designed for the Super–Kamiokande experiment. Vertex reconstruction relies primarily on timing information from a relative handful of tubes selected from the edge of the Cherenkov ring. The Super–Kamiokande PMT's exhibit a much tighter transit time distribution ($\sigma \sim 3\,$ns) than those of the earlier Kamiokande II experiment ($\sigma \sim 10\,$ns, with a pathological, double-peaked structure).[3] Hence we expect considerably better vertex resolution with 20% Super–Kamiokande photocathode coverage than a naive comparison with Kamiokande II would suggest: perhaps 45 cm for single-ring, sub-GeV events.

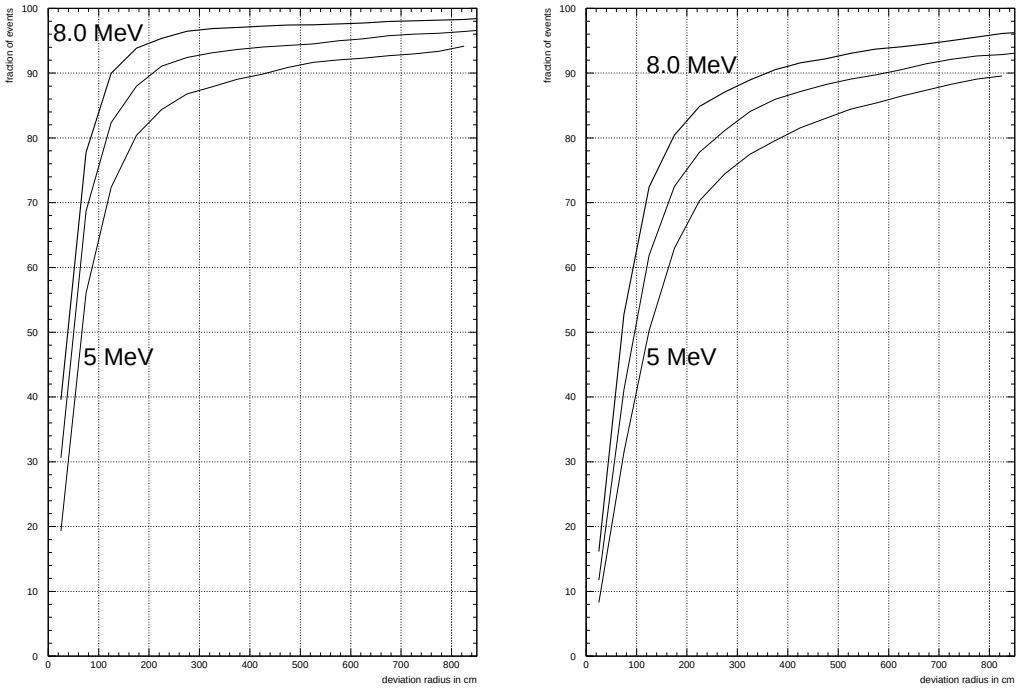

Figure 12: Monte Carlo study of vertex resolution with 40% (left) and 20% (right) inner PMT coverage. The vertical scale shows the fraction of events reconstructed inside a sphere around the true interaction vertex, the horizontal scale is the radius of that sphere. The three lines are for different regions of reconstructed energy (in 1.5 MeV steps).

6.1.3 Angular resolution

The directional resolution for single-ring, sub-GeV events in Super–Kamiokande is approximately 3°, compared to 4° for Kamiokande II. As even the Kamiokande II resolution much smaller than typical neutrino–lepton scattering angles, the transverse momentum imparted to nucleon decay products by Fermi momentum, and stochastic variations in the evolution of low-energy electromagnetic showers (for solar neutrinos), this small loss of pointing accuracy is unimportant.

The angular distribution of neutrino-induced upward-muons is peaked near the horizon, meaning these rare events must be separated from a background of much more abundant near-horizontal *downward*-going muons. Hence, the most important consequence of reduced photocathode coverage for the upward-muon analysis is potential loss of angular resolution and any resulting contamination from near-horizontal cosmic-rays.

With full photocathode coverage, the average parent neutrino angular resolution for upward-going muons satisfying the 7 m path-length criterion was 4.1°,[33] however the estimated contribution from intrinsic detector resolution was only 1.4°.

While detailed studies are under way, a preliminary simulation suggests a modest change in the angular resolution for energetic, entering muons from 1.4°(40%) to 1.9°(20%). We can also place an upper limit on the expected resolution by examining the perfomance of Kamiokande III.

The intrinsic resolution for reconstruction of upward-going muons with length > 7 m in Kamiokande III was 2.1°.[34] However, the PMT density per unit solid angle ($\sim 5537/4\pi$) will be about six times as high in Super–Kamiokande, even with 20% photocathode coverage. Upward-going muons in Super–Kamiokande will have more hit PMT's per event than Kamiokande, and also a much longer lever arm to constrain the parameters of the muon track. The 2.1° angular resolution of Kamiokande is therefore an upper limit on the loss of angular resolution in a half-density detector. With a fully-repaired outer detector, it seems likely that improved fits for through-going upward muons can be obtained by incorporating OD data into revised fitting algorithms. This effort, already underway, may eventually recover most, if not all, of the angular resolution lost due to the inner detector.

6.1.4 Particle identification

Particle identification relies principally on the sharpness of the Cherenkov hit pattern to distinguish showering and non-showering rings. For visible energies below a few hundred MeV, the opening angle of the Cherenkov ring provides additional information. At 40% photocathode coverage, the estimated probability of misidentifying a single-ring sub-GeV muon (electron) is $0.5 \pm 0.1\%$ ($0.7 \pm 0.1\%$).[1] Comparison of the predicted muon and electron hit patterns with an observed ring is ultimately performed by a maximum likelihood fit of all phototubes within a 70° cone about the ring direction. Since the number of "samples" available to this fit will decrease by a factor of two with 20% pho-

tocathode coverage, it can be expected that particle identification will worsen somewhat. In the Kamiokande II experiment, the estimated sub-GeV misidentification probability was $1.4 \pm 0.7\%$. As discussed, particle identification is influenced by not only raw photocathode coverage but also geometrical considerations (particle misidentification in the small 1-kton detector at KEK is approximately twice as large as in Super–Kamiokande, even though both have 40% coverage), so we expect Super–Kamiokande's particle misidentification probability with 20% photocathode coverage will be about 1%.

6.1.5 Ring-finding

The most challenging task in the reconstruction of complex events is the topological search for multiple Cherenkov rings. This procedure was the subject of considerable development work even before the November 12 incident. Some loss of performance is to be expected, since the number of points at which the Cherenkov light pattern is sampled is critical to this procedure. Comparisons to Kamiokande II are difficult, since in that experiment rings were identified by visual scanning rather than an automated algorithm.

A preliminary study, using Monte Carlo data, has been performed to assess the effect of reduced photocathode coverage on ring-finding (see Figure 13). The simplest benchmark for the ring-finding algorithm is tagging of π^0, which requires identifying both rings and correctly measuring their individual energies to reconstruct the invariant mass. Using a relatively small sample of simulated neutral-current atmospheric neutrino interactions containing π^0, the overall efficiency for π^0 identification drops from $50.2 \pm 3.2\%$ at full photocathode coverage to $46.0 \pm 3.2\%$ for half photocathode coverage. Only minor retuning of the algorithm to reflect the change in light collection was performed. This loss of efficiency is noticeable, but not large; it may be recoverable (at least in part) by optimization for reduced coverage and/or future improvements to the algorithm itself.

6.1.6 Energy/momentum resolution

Energy/momentum resolution is most critical to nucleon decay searches and above all, solar neutrino studies. For showering particles, the momentum resolution is mainly determined by the statistical error on the number of photoelectrons collected (for high-energy data) or the number of PMT hits (for low-energy data). Figure 14 shows the energy resolution as a function of true electron energy in the region of interest for solar neutrinos. While the energy resolution is degraded with less PMT coverage, it still allows the resolution of a oscillation minimum from quasi-vacuum solutions, given enough statistical accuracy. To take advantage of this improved accuracy, however, a better energy calibration is also required. Using the electron linear accelerator, Super–Kamiokande (at 40% coverage) was able to calibrate the energy scale to 0.64%. The limiting factors are time- and directional dependences most likely caused by a position and time-dependence of the photon attenuation length in water. The rebuilt

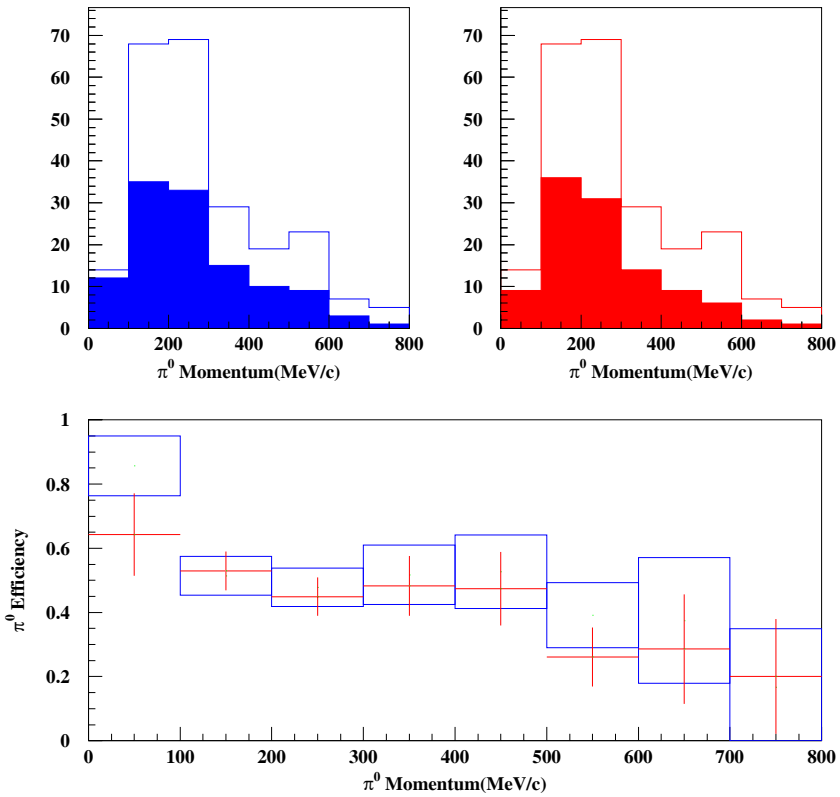

Figure 13: Preliminary comparison of π^0 identification for 40% (blue) and 20% (red) photocathode coverage. The upper figures show the number of generated (unfilled histogram) and reconstructed (filled) π^0 in a simulated atmospheric neutrino neutral-current data sample. The bottom figure shows the efficiency as a function of π^0 momentum. Averaging over all momenta, the π^0 identification efficiency is $50.2 \pm 3.2\%$ for 40% coverage and $46.0 \pm 3.2\%$ for 20% coverage.

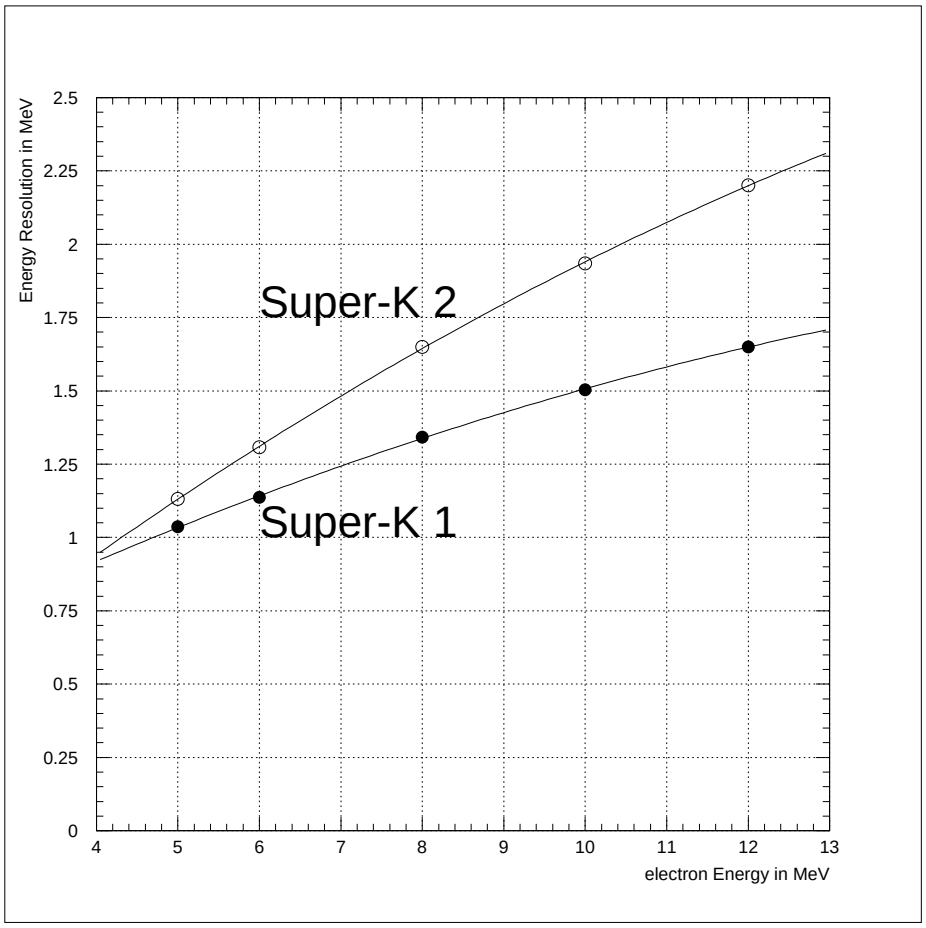

Figure 14: Energy resolution with 40% (filled circles) and 20% (open circles) PMT coverage.

Super–Kamiokande will be equipped with a new system of *in situ* laser beams installed during the recent maintenance, which will measure Rayleigh and Mie scattering as well as absorption as a function of wavelength, position and direction. This detailed information will allow us to improve the accuracy of the energy calibration to the required level.

For higher-energy events (nucleon decays, atmospheric neutrinos, and the KEK beam), we can simply estimate the relative energy resolution, and also compare to Kamiokande II. The undamaged detector's showering energy resolution can be described by[1]

$$\sigma_E^{40\%}/E = 0.5\% + 2.5\%/\sqrt{E/\mathrm{GeV}}.$$

Naively, one would expect halved photocathode coverage to translate into a

factor of two inside the square-root:

$$\sigma_E^{20\%}/E \approx 0.5\% + 2.5\%/\sqrt{E/2\,\mathrm{GeV}} = 0.5\% + 3.5\%/\sqrt{E/\mathrm{GeV}}.$$

In fact, this estimate is virtually identical to the quoted energy resolution of the Kamiokande II experiment:[2]

$$\sigma_E^{20\%}/E = 4\%/\sqrt{E/\mathrm{GeV}}.$$

For muons, momentum is measured using the muon range and (for lower energies) Cherenkov opening angle, and therefore the relative momentum resolution σ_p/p depends only weakly on the muon momentum. For the undamaged, 40% photocathode detector, this resolution is:[1]

$$\sigma_p^{40\%}/p = 3\%,$$

while for Kamiokande II:[2]

$$\sigma_p^{20\%}/p = 4\%.$$

For both showers and muons, the expected loss of energy resolution is approximately 1%, too small to noticeably degrade any high-energy physics analysis. For comparison, the *systematic* uncertainty on the calibration of the absolute energy scale (not included in the estimates above) in this energy regime is ±2.5%.

6.2 Outer Detector

6.2.1 Overview

The outer detector serves three important functions in Super–Kamiokande and K2K:

- Selection of the fully-contained event sample,
- Selection of the partially-contained event sample, and
- Supplementing the fiducial volume for K2K interactions using time coincidence with the beam.

Unlike the lavishly outfitted inner detector, the outer detector was designed to do its job with a minimum of instrumentation. Its nominal complement of phototubes is only 1/6 that of the inner detector, and the outer detector's tubes are 8-inch diameter, with 1/6 the sensitive area of the inner detector's 20-inch tubes. To increase the outer detector's light collection economically, waveshifter plates are mounted on the tubes; even so, the effective photocathode coverage of the OD is only about 2%. The surfaces of the outer detector are lined with sheets of white Tyvek to reflect Cherenkov light from passing tracks toward a larger number of tubes.

Given the sparse population and role of the OD, the average photocathode coverage is less important than hermeticity and uniformity. The majority of

outer detector tubes which survived the incident are over 15 years old and were originally employed in the IMB-3 experiment. Their advanced age undoubtedly contributes to the higher observed rate of attrition among OD tubes compared to the inner detector: roughly 0.2% per month, prior to the Summer 2001 maintenance. The process of redeploying the survivors to create a reduced coverage outer detector would inevitably result in further wear and tear, and possible further attrition. The preliminary studies cited below assess the effect of a *uniform* reduction in outer detector coverage, and therefore represent an unrealistic "best case" scenario. In reality, the random nature of PMT attrition makes it a statistical certainty that some regions will be depopulated more than others, with the number and size of these "holes" growing over time.

The varied nature and enormous volume of the potential contamination, which comprises not only muons but also secondary pions, neutrons and gamma rays, make it difficult to simulate or quantify the effect of even a small outer detector inefficiency. We are extremely wary of jeopardizing the heretofore excellent quality of our data by resuming operation with an inadequate outer detector. Any significant change in data reduction efficiencies, or the emergence of some new source of background, would compromise future data and make it difficult or impossible to combine with existing samples; ultimately, even past results could be called into question, due to real or perceived inconsistencies.

6.2.2 Fully-contained selection

The unglamorous, workmanlike character of the outer detector belies its effectiveness and indispensible role in the larger experiment: outer detector data largely determines which events will have their inner detector signals analyzed. Through simple cuts on pulse-height, timing and topology, the outer detector can quickly and efficiently veto all but a handful of the million or so uninteresting cosmic ray triggers recorded in a given day, leaving a manageable sample of candidate events for labor- and CPU-intensive inner detector scanning and reconstruction. Since these selections are unbiased by direction, position, or inner detector performance, they ensure a homogeneous and robust data set for physics analysis.

The outer detector plays the primary role in selecting fully-contained nucleon decay and neutrino candidates; it performs this task with near perfect efficiency. The vast majority of background events surviving outer detector selection which must be removed by subsequent scanning are not entering at all, but rather due to flashing of tubes in the inner detector. The repetitive and unphysical light pattern of these events makes them more of an annoyance than a source of contamination. Even so, scanning is time-consuming, subject to potential bias, and dependent on the scanner's level of care and experience. As such, scanning is by its very nature irreproducible and cannot be applied to the much larger simulated data samples (which of course do not include flashing PMT's). The U.S. groups have invested considerable effort toward fully automating the data reduction process, by contributing software tools to identify and reject flashers. This effort has been well-invested, since the number of events requiring scanning

has now been reduced to a tiny fraction of the level at the start of the experiment, with no loss of efficiency.

In view of the difficulties raised by scanning, the continued reliability of the outer detector is essential. While it is possible, in principle, to identify entering background using inner detector data, this is undesirable for a host of reasons. First, it would imply a completely new philosophy of data selection; developing and implementing such a scheme and ensuring its consistency with previously analyzed data would be a major undertaking. Second, it would be prohibitively expensive in terms of computing; whereas selection based on the outer detector involves little more than counting photoelectrons, any inner detector selection would require the much more involved procedure of vertex and track reconstruction. Third, it would introduce a coupling of event selection and reconstruction which does not presently exist; since the fully contained sample is currently selected without reference to inner detector data, it is possible to control for systematic effects in the inner detector performance using events outside the nominal fiducial volume, without need to account for any possible bias on the vertex and direction of tracks imposed by the selection criteria.

6.2.3 Partially-contained selection

The OD also aids in separation of partially-contained neutrino events from the background of cosmic ray muons and other entering particles. Partially-contained events are a key component of the atmospheric neutrino sample used in the global oscillation analysis. The partially-contained sample is unique in that it is populated with 97% pure ν_μ charged-current interactions. In addition, these high-energy events comprise a major element of the $\nu_\mu \rightarrow \nu_{sterile}$ analysis (see Section 7.3). Proper separation of fully- and partially-contained interactions is essential in the search for the oscillation pattern as a function of L/E (see Section 7.3.2), since the neutrino energy cannot be estimated with any precision in events with exiting particles.

With a uniform half-density outer detector, the efficiency for retention of partially-contained events in the fiducial volume decreases by roughly 10%; background before the final scanning step increases by about 20%, requiring additional human scanning effort. Non-uniform loss of additional coverage due to attrition would further aggravate these difficulties; they are avoided altogether with a full-density outer detector, ensuring the quality and consistency of the final atmospheric neutrino sample.

6.2.4 K2K events in the outer detector

The OD allows study of additional samples of neutrino events from the K2K beam, using events in-time with the beam spill that have light in both the inner and outer detectors (representing either exiting or entering leptons), as well as events with light in the outer detector alone (representing interactions in the rock or in the OD itself). The existing K2K event sample contains 12 exiting, 10 entering, and 21 OD-only events, with a total expected background of only

1.6 events. Systematic errors on the expected rates are relatively large for these events, however; so far they have only been used to check stability of the far-detector neutrino event rate. We hope to decrease these systematics through better understanding of the outer detector response.

The quality of the K2K outer detector event sample would be significantly degraded with missing OD tubes (although it is fairly insensitive to the inner detector PMT configuration). With half-density PMT's, the background increases by a factor of about five, and signal efficiency decreases by approximately 10%. A full-density, well-calibrated outer detector is essential to use the K2K outer detector events in neutrino oscillation analysis of the beam.

7 Physics Program

7.1 The K2K Experiment

One of the most pressing motivations for an expeditious repair of the detector is completion of the K2K experiment. The goal of the K2K experiment is to test Super–Kamiokande's oscillation results using a beam of man-made neutrinos where the flux and composition of the beam have different systematics than the atmospheric neutrinos. The neutrinos are produced at the KEK 12 GeV PS and directed at the Super–Kamiokande detector in Mozumi, Japan. So far, the K2K experiment has accumulated approximately half of its allocated protons-on-target; one more year of running with a refurbished far detector would suffice to collect the other half. Because the peak energy of the K2K neutrino beam is 1 GeV, the detector performance for beam-induced neutrino interactions with 20% photocathode coverage should be almost identical to that with 40% coverage during the first half of the run.

There is an important time constraint for the restart of the K2K experiment. The KEK laboratory has already arranged to increase the running time during 2003 from the normal 6 months to the full year. After this time the KEK 12 GeV PS will begin a decommissioning phase as the KEK accelerator division staff begin their transition to the 50 GeV JHF PS project. For this reason, a timely resumption of the K2K experiment is vital.

At the end of 2001 the experiment had detected 134 beam-induced neutrino events. Of these, 56 events were reconstructed inside the fiducial volume. Assuming no neutrino oscillations, 80.6 events should have been detected in the fiducial volume. The probability that the 80.6 events could have fluctuated down to 56 events due to statistics alone is about 2%. On the other hand, if the suppression of the ν_μ flux is due to neutrino oscillation with maximal mixing, the data agree nicely with Super–Kamiokande's measured Δm^2 of $3 \times 10^{-3}\,\mathrm{eV}^2$; for that value, 52.4 events would be expected in the fiducial volume. Figure 16 shows a confidence interval based on the total number of events observed inside of the fiducial volume, overlaid with the Super–Kamiokande 90% confidence level allowed region.

As Figure 16 shows, the Super–Kamiokande allowed region already agrees

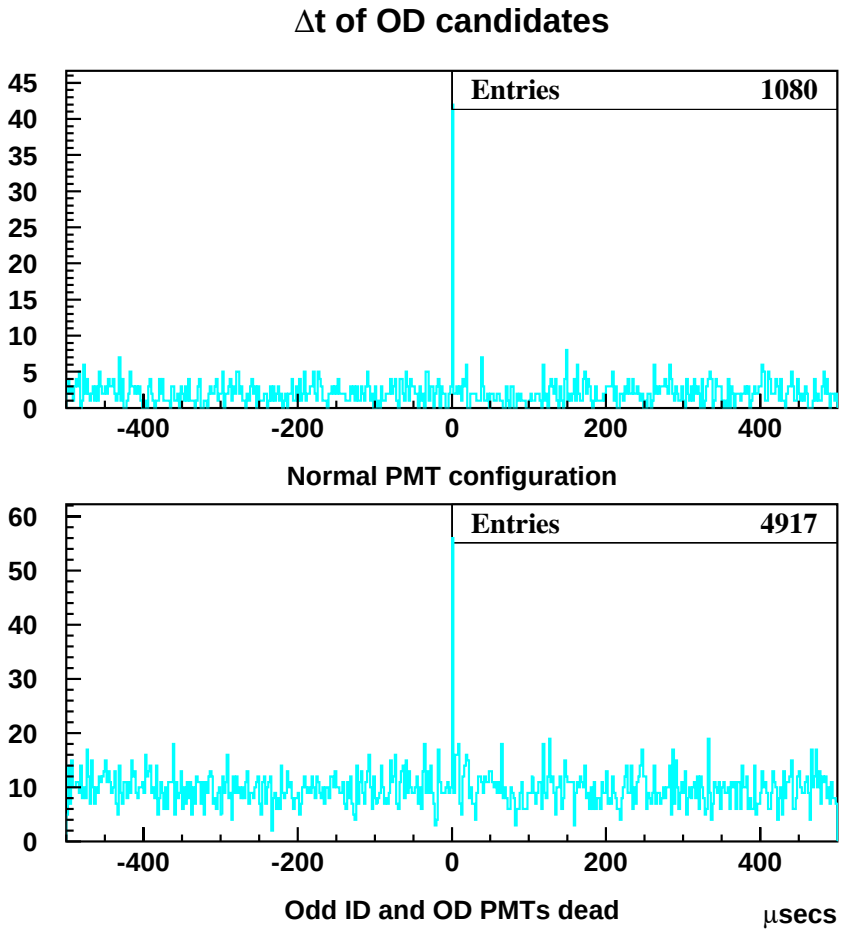

Figure 15: Time difference distributions for all K2K beam events in the OD, for full coverage (top), and with half OD tubes dead (bottom). The background level increases by a factor of about five.

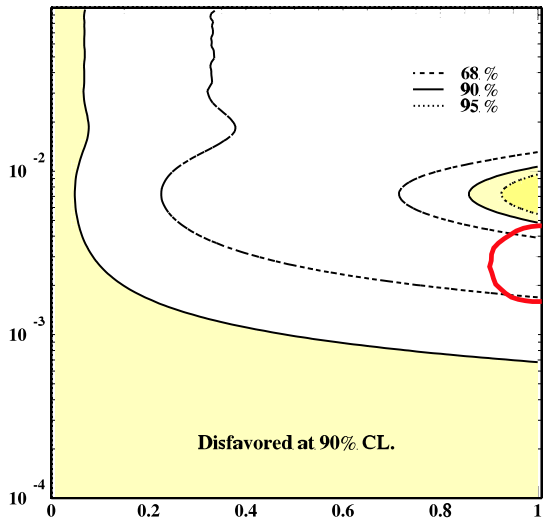

Figure 16: K2K allowed region based on the number of observed events inside of the Super–K fiducial volume. This analysis is based on a double sided Gaussian tail hypothesis test. The Super–Kamiokande 90% confidence level allowed region based on the global fit to all atmospheric neutrino data is overlaid for comparison.

very well with the measured K2K deficit. However tantalizing this result, the goal of the K2K experiment is to test the oscillation result with greater significance. To achieve this goal, more data is necessary. Figure 16 is based on only the total number of events observed. To obtain more significant results, and see positive proof of oscillations, an analysis sensitive to the energy-dependent spectral distortion must be applied.

Figure 17 shows the reconstructed neutrino energy of the 30 events with a single, muon-like ring detected inside the fiducial volume. These events are predominantly ν_μ quasi-elastic charged-current scattering for which the neutrino energy can be reconstructed based on the observed event kinematics. As the figure indicates, the data is consistent with oscillation for a Δm^2 of 3×10^{-3} eV^2, with the largest suppression appearing between 0.5 and 1.0 GeV. Work is now underway to obtain allowed oscillation contours based on this spectrum while accounting for the appropriate systematic errors.

Preliminary Monte Carlo studies have shown that, as of now, even spectral analysis of the K2K data is statistics limited. However, this will not be true if the current statistics are doubled and the experiment obtains its design luminosity of 10^{20} protons-on-target. We anticipate the significance of the single-ring quasi-elastic spectral analysis will be between $3 - 5\sigma$ with 10^{20} protons-on-target (compared to the current preliminary significance of approximately 2σ).

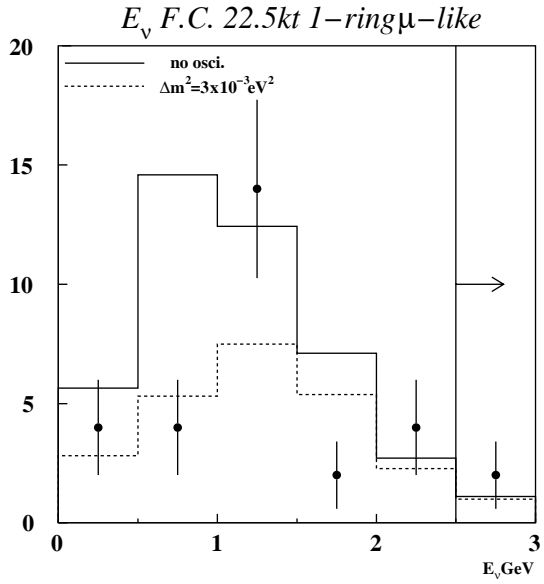

Figure 17: The reconstructed neutrino energy of single-ring muon-like events reconstructed in the fiducial volume of Super–Kamiokande. The solid line is the expectation for no oscillations and the dashed line is the expectation for oscillation with a Δm^2 of 3×10^{-3} eV^2.

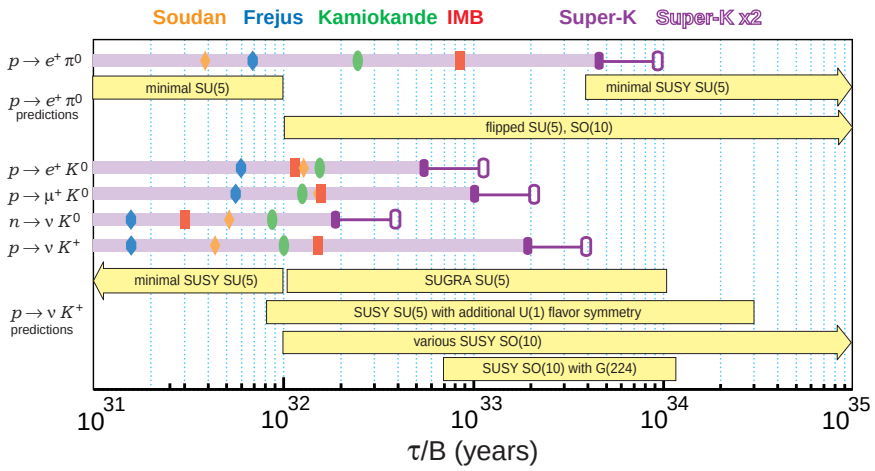

Figure 18: Selected experimental limits on nucleon lifetime compared to the ranges predicted by a variety of Grand Unified Theories. The hollow oval indicates the expected limit from doubling the current Super–Kamiokande exposure.

7.2 Nucleon Decay

7.2.1 Status and motivation

The Super–Kamiokande search for nucleon decay has not yielded any positive evidence, but the absence of nucleon decay, now extended into the decade between 10^{33} to 10^{34} years lifetime, has provided stringent constraints that must be addressed by any proposed Grand Unified Theory. In most GUT's, nucleon decay rates are naively predicted to be too large compared to our observational experience and some mechanism must be contrived to reduce them. The simplest theories, such as SU(5) and minimal SUSY SU(5) predict such short lifetimes that the they are already excluded (the two just mentioned, by IMB/Kamiokande and Super–Kamiokande respectively). Certain new theories have included features that make the lifetime arbitrarily long, for example separating quarks and leptons by extra spatial dimensions[4, 5]. Other theories involving extra-dimensions predict surprising new modes [14]. However, a large number of current GUT's that allow a finite nucleon lifetime predict decay rates not much beyond current limits[15, 16, 17]. Clearly the search for nucleon decay remains an extremely valuable discriminating experiment for understanding the fundamental nature of particles and forces.

Figure 18 shows selected nucleon lifetime limits compared to ranges of expectations from a variety of Grand Unified Theories[18, 19, 20, 21, 22, 23, 24, 25]. Further running of Super–Kamiokande is motivated by an expected doubling of the present nucleon decay sensitivity. While this additional sensitivity is not sufficient to exclude any of the theories listed, the additional exposure is probing and constraining these theories. Given the numerous predictions that the finite

nucleon lifetime may truly lie in this range, one can consider several possible outcomes from continued exposure. First, if a "golden" event or two is seen, then the approximate scale of the nucleon lifetime has been found, which can securely motivate the size of any next-generation detector. More importantly, whether the final state particles make energetic electromagnetic showers, as in the $e^+\pi^0$, or involve charged kaons, as in $\overline{\nu}K^+$, is a decisive question in the choice of the technology most suitable for any next generation detector. Simply observing nucleon decay will provide strong validation of the idea of Grand Unified Theories, and simply knowing the dominant branching mode is a significant discriminant between the wide variety of GUT's under consideration. Conversely, the non-observation of nucleon decay will further constrain the set of valid models, giving weight to those that allow for very long lifetimes, and casting doubt on those that require shorter lifetimes.

7.2.2 Nucleon-decay sensitivity

Since proton decay signatures yield fully-contained visible energy from 0.1 to 1 GeV, we anticipate that running the Super–Kamiokande inner detector with half of the original PMT coverage will be worthwhile. This will be 20% photocathode coverage, identical to Kamiokande and 4 times IMB, both of which were quite successful. Because of the large dimensions of the detector, 30 meters across inside, we profit not only from the fiducial mass of the detector, but also by projecting the Cherenkov rings over a wide area, thereby well separating them on the photosensor surface. The search for $p \rightarrow e^+\pi^0$ will be practically unaffected. The most significant impact of fewer PMT's, and one which is still under study, is that faint rings due to asymmetric π^0 decay, barely-above-threshold charged pions, and 6 MeV nuclear de-excitation, will become more difficult to detect.

An example of this is shown in Figure 19, which compares the same Monte Carlo event of $p \rightarrow \overline{\nu}K^+$ under two configurations of inner detector PMT's. The left panel shows the original configuration of 11146 photomultiplier tubes, and the right panel shows the new configuration with only half that number. The collapsed ring from the 236 MeV/c muon is sharp in both cases, and the Cherenkov angle of 35° should be readily reconstructed from the 2 nanosecond timing of the PMT's. To distinguish these events from the copious background of atmospheric ν_μ interactions, we search for the de-excitation of $^{15}N^*$ by a 6 MeV gamma ray[26, 27].

This gamma tag is possible because the K^+ is emitted below Cherenkov threshold, stops 15 cm away from the proton decay vertex, and decays with a mean lifetime of 12 ns. Therefore the prompt de-excitation of $^{15}N^*$ precedes the visible kaon decay by a time interval that can be resolved by the Super–Kamiokande detector. The signature is unique to proton decay when 8 or more hits are required in a sliding window 12 ns wide.[2] Figure 20 shows the number

[2]It is important to note that this analysis does not rely on the 6 MeV gamma ray *triggering* the detector; the delayed muon from kaon decay at rest produces ample light to trigger with 100% efficiency. Hence trigger threshold considerations with reduced photocathode coverage

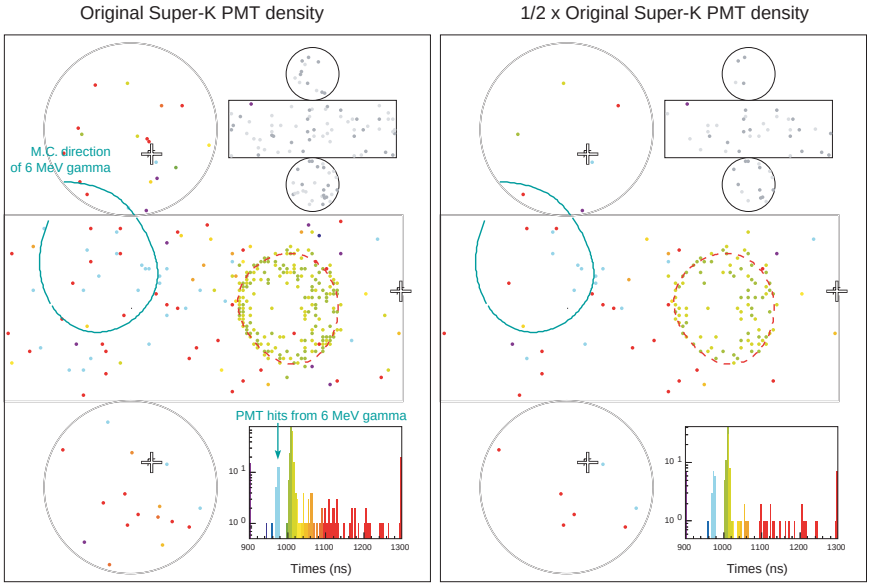

Figure 19: A comparison of the same Monte Carlo event of $p \to \overline{\nu} K^+$ with $K^+ \to \mu^+ \nu_\mu$ and de-excitation of $^{15}N^*$ to a 6 MeV gamma ray. The left panel shows the original configuration of 11146 photomultiplier tubes, and the right panel shows the new configuration with half that number. The gamma tag precedes the decay $K^+ \to \mu^+ \nu_\mu$ by 20 nanoseconds, as seen in the histograms of PMT hit times. The outer detector, in the upper corner of each event display, shows mostly out-of-time dark noise hits in a wider time window.

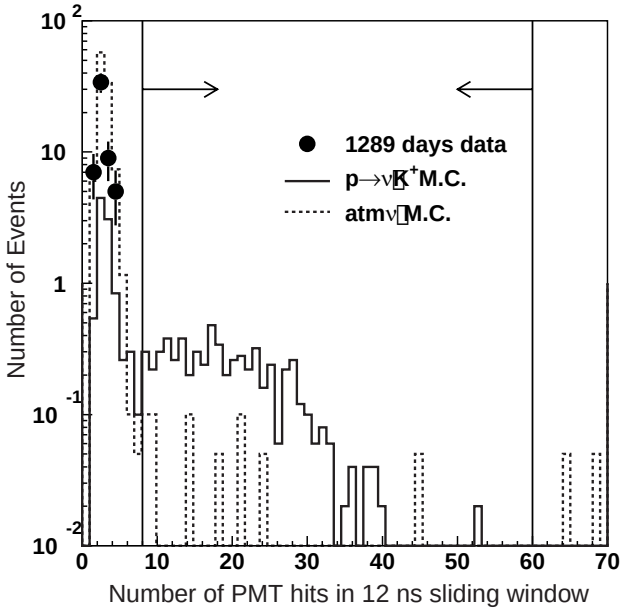

Figure 20: The distribution of early PMT hit times in a 12 ns sliding window that precedes the PMT hit times corresponding to the muon ring. The dashed curve shows that between 8 to 60 extra hits may be expected from the prompt gamma due to nuclear de-excitation during proton decay within ^{16}O. The solid curve shows that our atmospheric neutrino Monte Carlo predicts most neutrino events produce less than 8 hits for this algorithm. The data from the fully-analyzed 1289-day exposure are overlayed.

of hits found in the sliding window, considering proton decay Monte Carlo, atmospheric neutrino background Monte Carlo, and 1289 days of data. The signature from the gamma tag is expected to be between 8 and 60 hits (with the full complement of PMT's), with an efficiency $\times$ branching ratio of 8.8%. The background expected from atmospheric neutrinos is 0.5 events for the 1289-day sample. The lifetime limit for this method alone is $\tau/\beta > 10^{33}$ years (a preliminary result, updated from Ref. [27]); the combined limit including other channels now stands at 2×10^{33} years. It is expected that the efficiency, and perhaps the background, will be somewhat worse with half of the inner PMT's, but the signal stands out from the cut by tens of PMT hits, so we are confident that this analysis will continue to be effective. A detailed estimate of the new efficiency requires re-simulating the Monte Carlo samples, re-optimizing the vertex fitting algorithm and retuning the cuts.

are unimportant here.

7.2.3 $n\overline{n}$ oscillation

A recent paper has argued[6] that the $\Delta B = -2$ process of $n\overline{n}$ oscillation is a generic prediction of a large class of supersymmetric Grand Unified Theories with spontaneously-broken $B - L$ symmetry. In the case of supersymmetric unification based on the gauge group $SU(2)_L \times SU(2)_R \times SU(4)_c$, the $n\overline{n}$ lifetime is closely related to the neutrino masses via the See-Saw mechanism. Based on the inferred value of the largest neutrino mass from atmospheric oscillation data, the upper bound on the $n\overline{n}$ lifetime in such models appears to be $10^9 - 10^{10}$ seconds. Other models which propose new spacetime dimensions to explain neutrino oscillation also predict $n\overline{n}$ oscillation.[7]

Searches for $n\overline{n}$ oscillation in nuclei rely on the identifying the subsequent $N - \overline{n}$ annihilation products. In addition to final-state nuclear interactions of these secondaries, the rate of bound $n\overline{n}$ oscillation is strongly suppressed due in the nuclear potential well. The free $n\overline{n}$ lifetime of theoretical interest, $\tau_{n\overline{n}}$ is related to the corresponding lifetime in a nucleus A by the relation $\tau_A = (\tau_{n\overline{n}})^2 T_A$, where T_A is a suppression factor which can be calculated in a quantum mechanical potential model, or by a quantum field approach. A recent calculation finds, for ^{16}O, $T_{^{16}O} = 1.2\,\mathrm{fm}^{-1}$, or equivalently, $T_{^{16}O} = 3.6 \times 10^{23}\,\mathrm{sec}^{-1}$.[8] For comparison, the older calculation of Dover, *et al.*, predicts (more optimistically) $T_{^{16}O} = 1 \times 10^{23}\,\mathrm{sec}^{-1}$.[9] Adopting the more conservative value of $T_{^{16}O}$, the bound $n\overline{n}$ lifetime $\tau_{^{16}O}$ corresponds to a free $n\overline{n}$ lifetime $\tau_{n\overline{n}}$:

$$\tau_{n\overline{n}}/(10^8\,\mathrm{sec}) = 0.93\sqrt{\tau_{^{16}O}/(10^{32}\,\mathrm{yr})}.$$

Using an empirical model of the $N - \overline{n}$ annihilation products, the Kamiokande experiment set the limit $\tau_{^{16}O} > 4.3 \times 10^{31}$ yr (90% confidence level).[10] This analysis quoted an efficiency of 33% with an expected background rate of $1.0\,(\mathrm{kton\text{-}yr})^{-1}$. Assuming $T_{^{16}O} = 3.6 \times 10^{23}\,\mathrm{sec}^{-1}$, the Kamiokande measurement translates into a limit on the free $n\overline{n}$ lifetime $\tau_{n\overline{n}} > 6 \times 10^7$ sec, only slightly worse than the best limit from reactor-based searches: $\tau_{n\overline{n}} > 8.6 \times 10^7$ sec.[11] The Fréjus[12] and Soudan–II[13] experiments have also set limits comparable to, or slightly better than, the Kamiokande result.

A preliminary, as-yet unpublished, search for $n\overline{n}$ oscillation in Super–Kamiokande has yielded no evidence of a signal, and improves the Kamiokande limit on $\tau_{^{16}O}$ by approximately an order of magnitude. This in turn implies a factor ~ 3 improvement in Kamiokande's free $n\overline{n}$ lifetime limit.[3] Thus the result, when sufficiently mature for publication, should be the world's best, even after assuming the most pessimistic bound-neutron suppression factor found in the literature. For a ten-year Super–Kamiokande run (assuming, conservatively, the Kamiokande efficiency and background level) we can expect a 90% confidence level sensitivity $\tau_{^{16}O} \sim 10^{33}$ yr, equivalent to $\tau_{n\overline{n}} \sim 3 \times 10^8$ sec; a factor 3.5 improvement on the best reactor limit. Since this analysis is background limited,

[3] The analysis in [10] assumed the value $T_{^{16}O} = 10^{23}\,\mathrm{sec}^{-1}$, and quoted the free lifetime limit $\tau_{n\overline{n}} > 1.2 \times 10^8$ sec (90% confidence level). If this $T_{^{16}O}$ value is adopted, the $\tau_{n\overline{n}}$ sensitivity of a 10-year Super–Kamiokande run would be $\sim 6 \times 10^8$ sec.

beam data from the 1-kton near-detector at KEK will be invaluable in reducing the systematic uncertainty of the background subtraction.

7.3 Atmospheric Neutrinos

Super–Kamiokande's studies of atmospheric neutrinos have provided the most credible evidence for neutrino oscillation and neutrino mass. The significant experimental characteristics that made this possible are: (a) a wide range of neutrino energies, from 100 MeV to 1000 GeV; (b) a large variation in baselines, from 10 km to 10000 km; (c) a well-predicted initial ratio of electron and muon flavor neutrinos; (d) excellent particle identification in the detector; (e) up-down symmetry in the detector; (f) good energy and directional resolution; and (g) large data samples, with nearly 13,000 total atmospheric neutrinos analyzed. Exploiting these advantages, the data are finely binned in energy and angle during fitting, resulting in a precise estimate of the oscillation parameters. These same data can exclude alternate hypotheses such as neutrino decay and exotic oscillation processes with a high level of confidence. Particularly important are recent studies that exclude pure oscillation between muon neutrinos and sterile neutrinos, and limit the allowable admixture of sterile neutrinos to a relatively small fraction of the effect.

Additional exposure to the atmospheric beam will confirm and extend these measurements. The determination of oscillation parameters is now limited by systematic uncertainties. With further data from Super–Kamiokande and the near detectors at K2K, these systematics can be improved. However, other atmospheric neutrino studies discussed below are limited by the present statistics, and are crucial to establishing the detailed nature of neutrino oscillation.

We are confident that atmospheric neutrino studies can continue unimpaired with 50% of the inner detector PMT's. The 20% photocathode coverage is identical to Kamiokande, but as discussed in Section 6.1, Super–Kamiokande benefits from its large scale (which distributes Cherenkov rings over more pixels) and 20× greater fiducial mass. Energy resolution will degrade by about 1%, while position and direction resolution should be nearly unchanged. Particle misidentification between electron showers and muon tracks should be no worse than 2% as in Kamiokande (compared to 0.5–1% in Super–Kamiokande). The effects on multi-ring identification are still under study; however the relevant algorithms were under active development and improvement before the incident.

7.3.1 ν_τ appearance search

Analyses to identify a sample of charged-current ν_τ interactions are in progress and preliminary results have been reported at conferences.[29] Due to the complicated decay modes of the tau, as well as the large hadronic recoil multiplicity, it is not possible to isolate a very pure signal from the atmospheric neutrino beam, which extends to high energy, contains a large electron neutrino component, and includes the usual fraction of neutral-current interactions. Nevertheless, for the oscillation parameters implied by ν_μ disappearance measurements

(maximal mixing and $\Delta m^2 = 3 \times 10^{-3}\,\mathrm{eV}^2$), only upward-going neutrinos have sufficient energy for tau production ($E_{min} \sim 3.5$ GeV), as well as sufficiently long baseline for oscillation. Therefore, these analyses aim to create a sample enriched with charged-current ν_τ interactions and search for an excess in the upward direction.

To enhance the tau fraction, neural network and likelihood techniques based on visible energy, and the geometry of energy flow are under development. Since the ν_τ signatures are too complicated to reconstruct in detail even with the full 40% photocathode coverage, these techniques rely on a more global analysis of the light distribution and should be largely insensitive to any loss of ring-finding efficiency with reduced photocathode coverage. Assuming the measured oscillation parameters are correct and the atmospheric neutrino Monte Carlo accurately models the variety of neutrino interactions, an excess of ν_τ-enhanced events is observed in the upward direction. The current result is $92 \pm 35^{+15}_{-23}$ excess ν_τ events, where the first error is a statistical uncertainty from the fit, and the second is a systematic uncertainty due to the oscillation parameters: the allowed range of Δm^2 and the possible admixture of 8.7% ν_e as allowed by CHOOZ under a 3-flavor oscillation scenario. Doubling the statistics with further exposure should improve the result to 184 ± 50; even assuming no further reduction in systematic uncertainty, this represents a 2.7σ effect. Figure 21 shows the result for this hypothetical doubling of statistics from further running.

7.3.2 Search for the oscillation pattern

Although the global fit of all atmospheric neutrino data prefers nearly maximal $\nu_\mu \leftrightarrow \nu_\tau$ oscillation, the sin-squared form demanded by quantum mechanics has not yet been directly observed. Preliminary studies are attempting to isolate a subsample of the data with sufficient L/E resolution to exhibit this effect. Figure 22 shows one simulated data set reflecting the present four-year exposure (the actual data is kept in reserve until the analysis is fully developed). Observation of the first oscillation minimum will be statistically enhanced with doubled statistics.

7.4 Upward-going Muons

The upward-going muon events provide the highest energy sample of neutrinos available in Super–Kamiokande. Energetic muons travelling upward into the tank occur at the rate of about one event per day, after requiring a minimum track length (whether stopping or through-going) of 7 m (corresponding to minimum energy of about 1.6 GeV). The observed muons must be due to muon neutrinos interacting in the rock below the detector, since cosmic-ray muons are limited to the downward hemisphere and no other particle passing through the earth could produce a muon with sufficient energy to penetrate the detector. The parent neutrinos of these muons have typical energies around 10 GeV for stopping muons and 100 GeV for through–going muons.

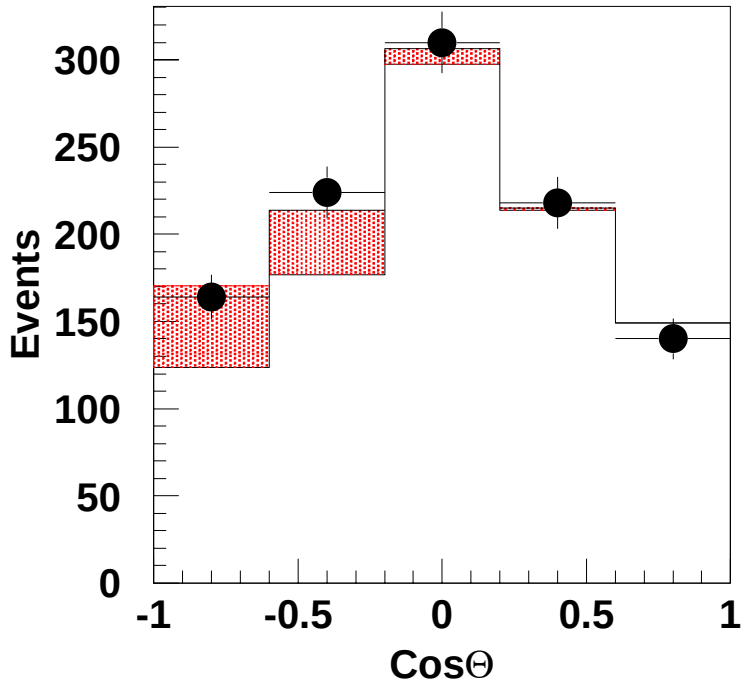

Figure 21: Zenith angle distribution of atmospheric neutrino events selected by a neural net analysis tuned to enhance the fraction of charged current ν_τ interactions. The plot shows the result expected after doubling the current 3.5 years of Super–Kamiokande exposure. The data points represent the number of events detected; the lower histogram represents the Monte Carlo prediction without accounting for ν_τ appearance; the filled histogram represents the expected additional events due to ν_τ appearance with the best fit oscillation parameters of $\sin^2 2\theta = 1$ and $\Delta m^2 = .003$ eV^2.

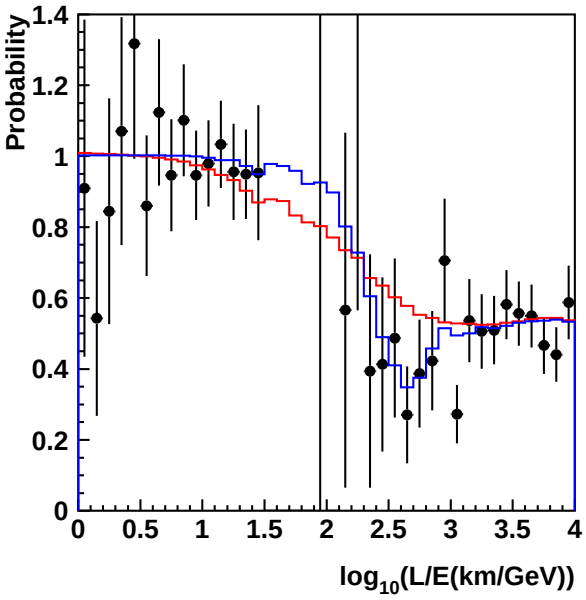

Figure 22: A simulated data set for 4 years exposure of Super–Kamiokande (equivalent to the current data sample), with events selected for good resolution in L/E. The data is compared to the standard two-flavor oscillation hypothesis, and a reference prediction based on decoherence that does not exhibit an oscillatory minimum.

These higher-energy neutrinos extend the experiment's L/E reach for oscillation studies by several decades and allow tests for energy-dependent phenomena such as $\nu_{sterile}$ matter effects and neutrino decay. By contrast, the majority of fully-contained neutrino events fall within a relatively narrow energy range. In addition, high energy neutrinos may be produced by astrophysical sources.[30]

Muons produce copious Cherenkov light in the inner detector, so reduction of photocathode coverage does not affect triggering for these events.

Downward, cosmic-ray muons near the horizon may be misidentified as upward-going, and likewise, upward, neutrino-induced muons near the horizon may be rejected as downward-going, but the number of downward muons so overwhelms the number of upward ones that leakage across the horizon does not cancel on average. Thus, neutrino-induced muon events in the angular region just below the horizon are contaminated by a background of cosmic-ray muons.

Reduced resolution implies that a wider angular region will be contaminated, and contamination in a given region will be larger than before; thus, the signal:noise ratio will decrease. In the past analysis, this contaminated region was $0 > \cos(\theta_z) > -0.05$.[32] The estimated 0.5° increase in angular resolution resulting from reduced photocathode coverage (see Section 6.1.3) should translate to a roughly 35% increase in the low level of present background. As in the past, azimuthal variation of the mountain overburden will allow any additional contamination to be measured and subtracted reliably. Hence we do not expect this slight increase of cosmic-ray background to adversely affect any physics analysis.

The expected $\sim 2^\circ$ muon resolution is modest compared to the overall 4.1° neutrino resolution of the undamaged detector. Hence any broadening of the neutrino angular resolution will be too small to affect oscillation or astrophysical analyses significantly.

7.4.1 Oscillation physics

Physics results from upward-going muons are primarily limited by statistics. We have shown in our analysis of $\nu_\mu \rightarrow \nu_{sterile}$ that the upward muon sample, with its much higher energy reach, exerts strong constraints on the various models considered. In addition, the upward muon sample provides some leverage on the lower end of the Δm^2 range in combined fits with the contained event samples.

An increasing upward muon sample will remain valuable to neutrino oscillation analyses for the forseeable future.

7.4.2 Neutrino astrophysics

Accumulation of additional upward muon data will allow us to refine and extend our search for astrophysical neutrino sources.[31] This is particularly important for sources which are periodic, intermittent or flaring (e.g., TeV gamma rays observed from Blazars); such sources are the norm in high-energy astrophysics. One such type of neutrino source is a gamma ray burster(GRB), which may

produce very narrow beams of neutrinos; temporal and directional correlation of upward-going muons with optical detection would have tremendous impact on the understanding of these puzzling phenomena.

7.4.3 Dark matter

Upward-going muon data from Super–Kamiokande have been used in an indirect search for dark matter in the form of Weakly Interacting Massive Particles (WIMPs). Data were tested for an excess (over expected atmospheric neutrino background) of high energy neutrino events from candidate regions where WIMP annihilations might be expected to occur, such as the Sun, the Galactic Center, and the core of the earth. No significant excesses were found, and upper limits were calculated.[35] These results are presently statistics-limited and accumulation of further data will permit significant improvement of the published limits.

7.5 Solar Neutrinos

7.5.1 Present status

Water Cherenkov detectors, and in particular Super–Kamiokande, have had a very successful history in solar neutrino research. Even though only the relatively high-energy ^{8}B neutrinos (and *hep* neutrinos) are detectable, a wealth of information about solar neutrinos has been obtained. The strongly forward-peaked angular distribution of elastic neutrino-electron scattering provides clear evidence that the measured interactions indeed come from the sun. At the same time, this distribution allows statistical separation of the background from the solar signal, so it is not necessary to rely on a calculation of various potential backgrounds. The elastic scattering cross section is well known, so no neutrino source calibrations are required. Combined with the beautiful data of the SNO experiment,[28] Super–Kamiokande's precision elastic scattering measurements have provided the best evidence to date that the solar neutrino flux deficit is due to oscillation rather than more mundane effects.

Since Super–Kamiokande records solar neutrino events in real time, potential time variations of the solar neutrino flux can be studied. Measurements over half a solar cycle found no significant changes in the overall ^{8}B flux, while the yearly change of the flux (due to the change of distance between sun and detector) has been observed. No excesses (or deficiencies) due to neutrino flavor oscillations (or other causes) were observed. The possibility of daily variations in the interaction rate (which can occur due to neutrino flavor oscillations) was investigated with high precision: no significant variations were found.

Through a precision study of the recoil electron spectrum, a search was conducted for distortions of the neutrino spectrum due to neutrino flavor oscillations, but once again no significant distortions were found.

Because elastic neutrino-electron scattering is sensitive to μ- and τ-type neutrinos as well, the presence of other neutrino flavors in the solar neutrino flux

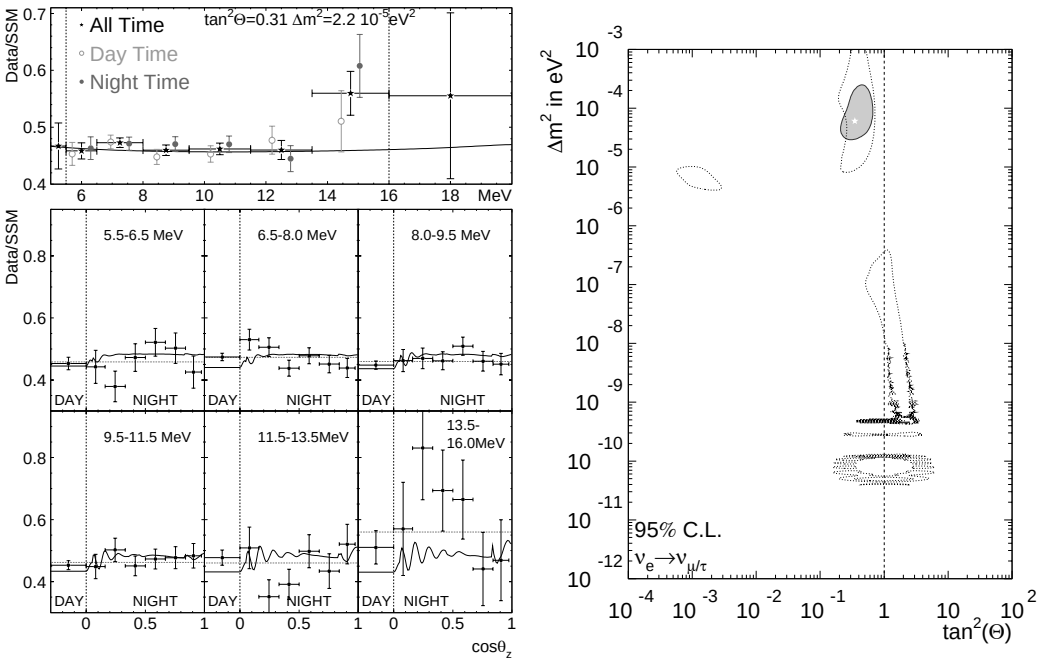

Figure 23: Super–Kamiokande zenith angle spectrum [left] and remaining allowed regions (at 95%) of mass^2 difference (Δm^2) and mixing angle ($\tan\theta$) [right] for two-flavor neutrino oscillations with Super–Kamiokande data (grey area) and without (inside dotted lines). Only one region remains (the so-called "Large Mixing Angle" solution) at about 95% C.L. The top panel on the left shows the measured spectrum, the lower panels the solar zenith angle (θ_z) variations in six energy regions. Superimposed as a curved line is a representative LMA oscillation prediction.

can be detected if the e-type flux is inferred from the electron-only rate measurements of SNO or Homestake. Super–Kamiokande found a more than 3σ excess from this measured pure-ν_e flux in its elastic scattering rate, strongly suggesting neutrino flavor oscillations. The experiment's precision measurements of daily variations and spectral distortions (or more precisely the lack thereof) confines the solar neutrino oscillation parameters to the Large Mixing Angle solution (LMA) at about the 95% C.L.(see Figure 23).

7.5.2 Motivation for continued solar neutrino studies

While Super–Kamiokande's measurement of the neutrino interaction rate is now limited by systematic uncertainties, the precision of time variation and spectral distortion can still be improved upon by continued exposure. So far, Super–Kamiokande has monitored the ^{8}B flux for about 5 years (about half a solar cycle), while observation over a full cycle will yield additional information about the stability (e.g., temperature and pressure) of the core of the sun. The daily variation of the high energy tail of ^{8}B neutrinos (i.e., those above 11 MeV) gives the greatest sensitivity to LMA oscillations. Unfortunately, the statistical uncertainty for this tail is the largest (see Figure 23) of all the accessible energy regions. Consequently, continued, long-term observation of this high energy tail will further constrain LMA oscillations. Moreover, the yearly variation of the same high energy neutrinos will serve to place more stringent limits on vacuum oscillation parameters (currently marginally allowed at the 92% C.L.). At the same time, those vacuum oscillation parameters predict spectral distortions at about the same energy and can therefore also be constrained in this manner by prolonged exposure.

Due to the high effective threshold of the SNO experiment ($T_e > 6.75$ MeV corresponds to about 9 MeV in Super–Kamiokande), an elastic scattering rate with a high threshold provides a neutral current probe independent of spectral distortions (pointed out by Lisi et al.). Currently, the statistical significance of an enhanced neutral current signal is slightly above 3σ. Although the significance is currently dominated by SNO's uncertainties, these are likely to decrease in the future. Another measurement of the flux with reduced systematics (due to energy scale) can therefore increase the precision of the elastic scattering neutral current signal, hopefully allowing a spectral analysis of the neutral current, which the deuterium neutral cross section from SNO cannot provide.

In summary, our largest statistical uncertainty in the recoil electron spectrum occurs in its high energy tail. Oscillation solutions that are not yet excluded can induce time variations and spectral distortions in this tail, so without question an improvement in statistical accuracy there will yield additional information about solar neutrino oscillations. At the same time, a high energy threshold elastic scattering rate measurement might yield spectral information about the neutral current-induced ^{8}B neutrino interaction rate.

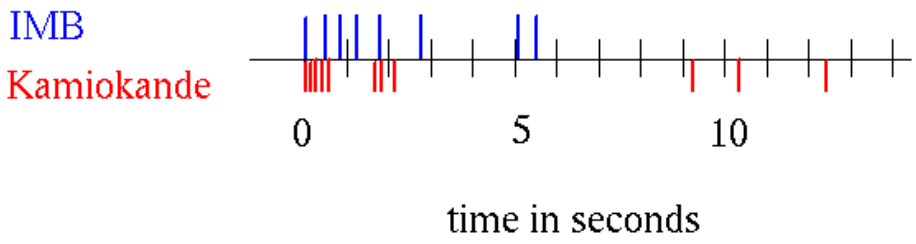

Figure 24: Time structure of 1987A neutrino events observed by water Cherenkov detectors in the U.S. and Japan.

7.6 Supernova Neutrinos

On February 23, 1987, the first radiation from the explosion of a blue supergiant in the Large Magellanic Cloud with the unwieldy name of Sanduleak -69° 202 reached Earth and became known as supernova 1987A. An estimated 3 ± 1 supernova occur in our galaxy and its satellites every century but the vast majority of stars are obscured by dust, making SN1987A the first supernova observed near our galaxy in almost 400 years. The last visible supernova was noted by Kepler in the year 1604. Estimates suggest that less than 10% of the galaxy is visible to the naked eye, making it quite likely that the next galactic supernova will be obscured as well; but the dust which obscures starlight is transparent to neutrinos.

Three hours before the light from SN1987A was observed, a handful of inverse beta decays:

$$\overline{\nu}_e + p \rightarrow e^+ + n, \tag{1}$$

were detected by two water Cherenkov detectors: Kamiokande II in Japan and IMB in the U.S. These events provided the first direct information from the interior of a stellar explosion, giving information about the temperature as well as the time evolution of the star immediately following the collapse of the core into a neutron star. The handful of events summarized in Figure 24 have been the topic of hundreds of publications during the decade and a half since SN1987A was observed.

Although the resulting events did not provide detailed information concerning the burst, these observations nevertheless energized the field of neutrino astrophysics. Both theorists and experimentalists alike hope to see the neutrino signal from the next galactic supernova. With Super–Kamiokande back in operation when the supernova's neutrino wave sweeps across the earth, we can gather information about nucleosynthesis, degenerate states of matter, shock wave stall and reheating, neutrino flavor mixing, neutrino mass, stellar atmospherics, and general relativity. Super–Kamiokande's physics potential in the wake of a galactic supernova is enormous. It is vital that the detector be repaired and back

Table 2: The total number of events expected in Super–Kamiokande with 20% photocathode coverage as compared with other detectors, either under construction (*) or running (**), for a supernova at 10 kpc.

Detector	Method	Mass	Events
Super–Kamiokande (*)	water Cherenkov	22.5 kiloton	∼7,750
SNO (**)	water Cherenkov	1 kiloton	∼1,000
KamLAND (**)	scintillation	1 kiloton	∼500
Borexino (*)	scintillation	1 kiloton	∼200
LVD (**)	scintillation	0.5 kiloton	∼200

online when it occurs.

7.6.1 Supernova neutrino signals

Super–Kamiokande's large mass compared to other existing facilities means that its data sample will easily outnumber that of all other detectors combined. This will remain the case until another large-scale nucleon decay and neutrino detector sensitive to supernova neutrinos is constructed. Table 2 summarizes the expected number of events observed for a supernova at 10 kpc.

For an explosion at the center of our galaxy, we expect ∼300 events per kiloton of water. Super–Kamiokande is sensitive to three main neutrino signals:

1. Weakly forward inverse beta decay events: ∼93%
2. Neutral current events involving ^{16}O: ∼4%, and
3. Directional elastic scattering events from $\nu_x + e^-$ and $\overline{\nu}_x + e^-$: ∼3%.

Each one of these modes will yield unique information. To illustrate, we will assume a type II supernova explosion 10 kpc (32,600 light-years) distant from Earth. This is a little past the galactic center and includes about half of the stars in the galaxy.

Inverse beta decay

From a type II supernova at 10 kpc, Super–Kamiokande will measure ∼7,200 inverse beta decay events, providing a relatively fine-grained energy spectrum and time evolution of the burst. This will allow a view of the dynamics and processes at work during the gravitational core collapse and resulting explosion.

Neutral current from ^{16}O

In 1996, Langanke, Vogel, and Kolbe[36] pointed out the following neutral current reaction:

$$\nu_x + {}^{16}O \rightarrow \nu_x + \gamma + X \tag{2}$$

where ν_x can be any of $\nu_\mu, \overline{\nu}_\mu, \nu_\tau$, or $\overline{\nu}_\tau$.

Higher energy supernova neutrinos can boost ^{16}O nuclei into the nuclear continuum, ejecting a nucleon and leaving either ^{15}O or ^{15}N in an excited nuclear

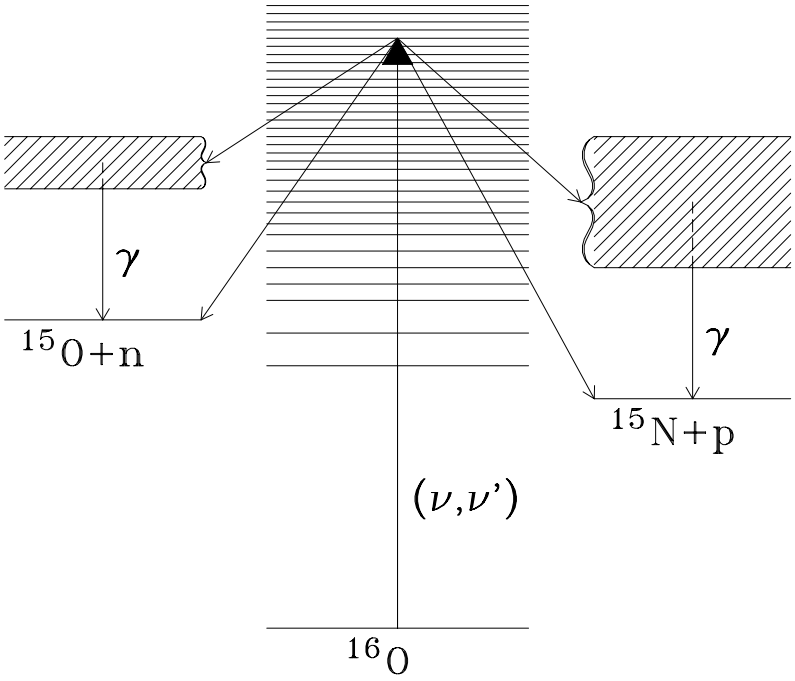

Figure 25: Nuclear energy level schematic for the neutral current process involving ^{16}O suggested by Langanke, Vogel, and Kolbe.[36]

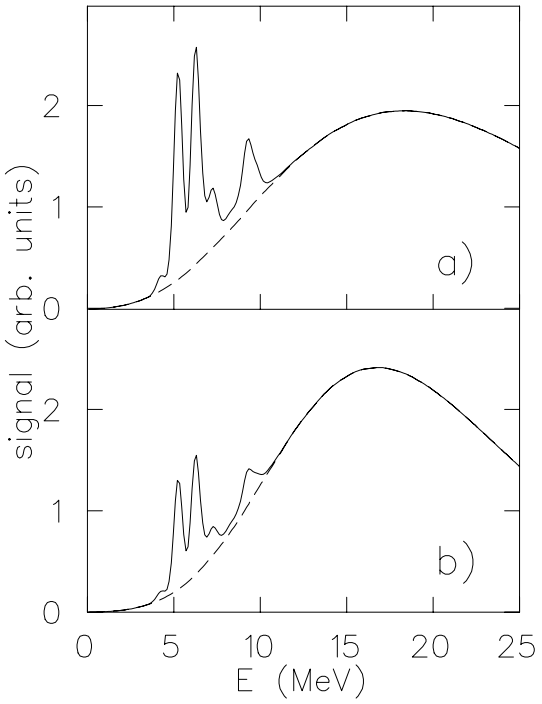

Figure 26: Energy spectrum showing the peaks produced by the neutral current process involving ^{16}O. The two plots assume differing average neutrino temperatures (top plot: T = 8 MeV, bottom: T = 6.3 MeV), indicating the sensitivity of this measurement.[36]

state. These decay in turn, emitting gamma rays in the process. Figure 25 shows the energy levels which generate these gamma rays. For a supernova at 10 kpc, this reaction will yield some 310 events in Super–Kamiokande.

These neutral current reactions produce mono-energetic photons in the energy range 5 $\rightarrow$ 10 MeV; the resulting events are easily identified, as shown in Figure 26. Since boosting ^{16}O into the nuclear continuum requires significant energy, these reactions are extremely sensitive to the temperature of the neutrino spectrum. Consequently, observation of these sharp energy lines in an otherwise smooth energy spectrum should tell us something about the stellar conditions which produced the heavy neutrino flavors as well as provide a handle on any flavor oscillations occurring in flight.

Elastic scattering

Neutrino elastic scattering should provide about 240 events in the half-coverage detector. These interactions preserve the direction of the incoming neutrinos and will allow us to determine the supernova's location in the sky. Using these events we could determine the position of the burst to within about $\pm 2^\circ$; this will allow astronomers to bring a variety of highly sensitive ground- and space-based

instruments to bear on the new supernova, facilitating collection of additional unique data about both the progenitor star and the intervening interstellar medium. For the past three years the Hubble Space Telescope has had an official Target of Opportunity proposal pre-approved in anticipation of just such a time-sensitive, neutrino-triggered alert; Super-Kamiokande is the leading member of the SNEWS (SuperNova Early Warning System) inter-experiment network conceived to provide it.

7.6.2 Black hole formation

Observationally, we know that massive stars end their lives as supernovae. Theoretically, we believe they can also form black holes; roughly half the stars whose cores collapse may end up as black holes. While this would seem to preclude the detection of neutrinos, black holes form *after* neutrino generation is under way. As a consequence, the high-statistics samples available to Super–K allow a search for direct evidence of black hole formation.

Under normal conditions (as was experimentally verified with SN1987A), the burst of neutrinos from a supernova should gradually trail off over the course of many seconds. However, if a black hole forms in the middle of a supernova explosion, the neutrino flux will be abruptly cut off as the event horizon rises up to swallow the neutrinosphere of the imploding star. Observation of such a cutoff in the supernova neutrino time structure will provide "direct" evidence for the birth of a black hole and would be incontrovertible evidence of their existence.

The use of black hole formation during a supernova has been proposed to directly determine the mass of the electron neutrino at the eV scale. The technique exploits the expected sharp cutoff in supernova neutrino luminosity discussed above. It predicts that Super–K could determine the mass of the ν_e down to 1.8 eV by measuring the relationship between energy and arrival time of ν_e's straggling in after cutoff (see Figure 27). Further, because of mixing between the neutrino flavors, direct mass limits on ν_μ and ν_τ are also possible.[37]

While terrestrial experiments will likely set more stringent limits on the ν_e mass, this exercise shows how measurements can be made using the precise neutrino-based "time zero" provided by black hole formation. This technique, especially in combination with other astronomical observations, can produce many other interesting and unique results.

7.6.3 Photocathode coverage

All the numbers quoted above assume a detector with 20% photocathode coverage of the inner volume. Table 3 shows how this half-density detector's performance compares to the original coverage.

Since reducing the density of PMT's raises the detector's sensitivity threshold (see Section 6.1), not surprisingly the largest effect on supernova physics is for the particularly low-energy gammas produced by ^{16}O excitation. However, the remaining ^{16}O events will still be easily identified, and so the detector's

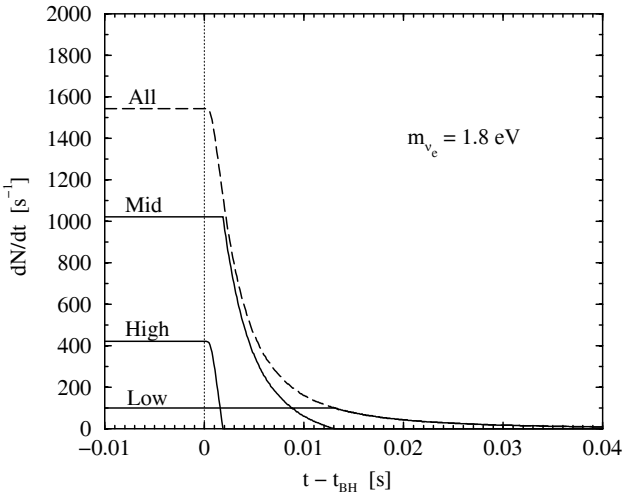

Figure 27: Neutrino data is broken up by energy range to provide a sharp "time zero" for the black hole formation (high energy) and well-defined delayed arrival times (middle energy). This delay is directly related to the mass of the ν_e.[37]

Table 3: Super–Kamiokande performance during a galactic supernova for different PMT densities.

PMT Coverage (%)	Number of Inverse β's (at 10 kpc)	Number of ^{16}O Events (at 10 kpc)	Number of Elastic Scatters (at 10 kpc)	ν_e Mass Limit (eV)
40	8,000	700	300	1.8
20	7,200	310	240	1.8

physics reach should not be significantly compromised. From the point of view of supernova physics, returning the detector to operation as quickly as possible, even with 20% photocathode coverage, is the most essential task.

8 The Future – JHF

8.1 Motivation and Status

Super–Kamiokande's atmospheric neutrino results and solar neutrino data (in combination with the Sudbury experiment) have established the reality of neutrino oscillation conclusively. Study of neutrino mass splittings and mixing angles, an entirely new sector of physics outside the Standard Model as understood until a few years ago, has already revealed surprises. The atmospheric mixing angle (θ_{23}) is apparently almost maximal, very near $\pi/4$; indeed, the weak neutrino eigenstates ν_μ and ν_τ have no well-defined masses at all but are almost equal mixtures of two mass eigenstates. Solar neutrino data increasingly favors a large mixing angles (θ_{12}). Yet the CHOOZ experiment has demonstrated that the third mixing angle (θ_{13}) is relatively small, $\sin^2 2\theta_{13} < 10\%$. Clearly the leptonic mixings bear little resemblance those of the quarks – a new and fundamental revelation. The three neutrinos are either nearly degenerate at some unknown common mass value below about 1 eV, or exhibit a hierarchy which strongly suggests a new, large "see-saw" mass scale close to the extrapolated point of coupling unification. In this case, neutrinos are Majorana particles and neutrinoless double β-decay should occur. If the LSND neutrino oscillation result is confirmed, it implies a fourth neutrino species, or the equally unexpected non-equivalence of neutrino and anti-neutrino masses; in either case, precision investigation of neutrino oscillation becomes even more essential.

At a minimum, two mixing parameters remain to be pinned down: the small mixing angle θ_{13} and the leptonic analog of the hadronic CP-violating phase, δ_{CP}. Establishing some lower bound on θ_{13} is the first priority, since if this angle is less than a degree ($\sin^2 2\theta_{13} < 10^{-3}$), measurement of δ_{CP} will require a neutrino factory, if it is observable at all. Likewise, finite θ_{13} is required to determine the order of the mass hierarchy ($\mathrm{sgn}\,\Delta m^2_{13}$) via matter effects at accelerator energies.

These physics imperatives have motivated study of long-baseline experiments using extremely intense "superbeams" produced by high-power proton sources. Large proton luminosities and neutrino fluxes are required to extend sensitivity to the small mixing angle θ_{13} significantly beyond CHOOZ. Disappearance experiments cannot achieve the level of precision required, hence the ν_e content of the beams must be carefully controlled and a large far detector with good ν_e/ν_μ discrimination is required to detect a small appearance signal with acceptable background.

The furthest advanced and most detailed of these superbeam studies is the JHF-Kamioka long-baseline proposal.[38] As described below, in Phase I of this

experiment the 0.75 MW[4] 50 GeV proton synchrotron at JHF (JAERI) would direct a narrow-band, ∼700 MeV off-axis beam of ν_μ, designed to contain only 0.2% ν_e contamination, 295 km to Super–Kamiokande. Using the measured performance of the (full) Super–Kamiokande detector and the well-established resolutions of existing reconstruction tools, a factor ~ 20 improvement on the CHOOZ $\sin^2 2\theta_{13}$ sensitivity is expected in a 5-year run. An order of magnitude improvement in the precision of $\sin^2 2\theta_{23}$ and Δm^2_{23} and a sensitive direct search for $\nu_\mu \to \nu_{sterile}$ oscillation using neutral current interactions are also planned.[5]

The 50 GeV proton synchrotron is under construction; the neutrino beamline's prospects for approval, with completion in early 2007, are considered good. As the most mature and compelling prospect for pursuing long-baseline oscillation physics beyond K2K, MINOS and the CERN-Gran Sasso experiments, the JHF-Kamioka project has generated strong interest from neutrino physicists in North America and Europe and an international collaboration will be formed to elaborate the technical design of the experiment some time in the coming year. One of the most attractive features of the JHF-Kamioka project is that it leverages the existing resources and scientific capital of Super–Kamiokande to launch a new, major experiment affordably and on a very competitive timetable. Recommissioning Super–Kamiokande is therefore not just a short-term investment to complete the experiment's *present* physics program; it is also an essential down-payment on a powerful and unique *future* program ripe with discovery potential, which could produce dramatic results at a modest incremental cost in a little over five years.

8.2 Off-Axis Neutrino Beam

The design of the neutrino beam is guided by the primary discovery channel of the experiment, namely detection of $\nu_\mu \to \nu_e$ oscillation via ν_e appearance at the level of a few per mille. To obtain a measurable signal, thousands of unoscillated ν_μ interactions must be collected. The linear rise of the neutrino cross-section with energy thus favors a high-energy beam. Background considerations, on the other hand, require the opposite – a low-energy beam – since both ν_e contamination from kaon decay in the beam and neutral-current background from misidentification in the far detector also increase sharply with energy. A typical wide-band neutrino beam, even one peaked around 1 GeV, includes a high-energy tail which contributes disproportionately to these backgrounds. The novel solution to these competing considerations is to place the far (and near) detector a few degrees off the axis of the beam. The kinematics of pion decay then produce a strong enhancement around a particular angle-dependent energy (chosen to maximize to the oscillation probability given Δm^2 and L), while strongly suppressing the ν_e component and high-energy tail of

[4] For comparison, the power of the 12 GeV KEK proton synchrotron used in K2K is only 0.005 MW; NUMI is 0.4 MW.

[5] A possible second phase of the experiment, using upgraded (4 MW) proton intensity and a hypothetical Mton-scale water detector would be sensitive to δ_{CP} over most of the parameter-space accessible to a neutrino factory.

the beam. As Figure 28 shows, the (useful) neutrino flux at the peak of such an off-axis beam (with maximum oscillation probability) is actually higher than at the peak of the wide-band, on-axis beam, further improving the signal to noise.

For the best possible characterization of the unoscillated neutrino beam (including ν_e contamination) and to measure the rate of neutral current background, two near detector facilities – one at the production source, as in K2K, and another 1-2 km downstream[6] are planned.

8.3 Super–Kamiokande as Far Detector

Super–Kamiokande, fully restored to its original sensitivity, is ideally suited to the requirements of a ν_e appearance experiment. The detector's large mass facilitates an experiment below 1 GeV, where the signal:noise is optimal but the cross-section is low. Most visible neutrino reactions at these energies are quasi-elastic, and therefore easily identified as either ν_μ- or ν_e-induced using the Cherenkov pattern and muon decays. For an appearance experiment, the particle identification criteria can be tightened to reduce lepton misidentification to a negligible level with only slight loss of efficiency for the signal. Another advantage of the narrow, off-axis beam tuned to the oscillation maximum is that approximately half the ν_μ oscillate to ν_τ which are then below charged-current threshold.

The remaining detector-related background arises from neutral current π^0 production. Production of secondary hadrons is largely suppressed by the relatively low-energy of the beam. Moreover, most π^0 produced are themselves low-energy and produce two distinct rings, excluding them as ν_e candidates. For the others, we have developed a specialized π^0 identification algorithm which searches single, showering events for the best direction and energy of a second ring candidate. For most ν_e quasi-elastic events with only a single primary electron, this second ring candidate is either coincident with the first ring, or very low energy; in either case the primary and secondary rings sum to an invariant mass close to zero. For π^0, however, the second ring candidate often corresponds to the missing γ, and the two rings reconstruct to a relatively large invariant mass, consistent with that of a π^0. After all selections, the total instrumental background from neutral currents and ν_μ charged-currents is reduced to the level of ν_e contamination in the beam; further improvements in the detector performance, while possible, would yield diminishing returns. The need for exceptional μ/e and π^0/e discrimination in the ν_e appearance search are a strong motivation for the eventual restoration of full inner-detector photocathode coverage, because the performance of pattern recognition algorithms (particle ID and ring-finding) depends strongly on the granularity with which the Cherenkov light pattern is sampled. This is clearly illustrated in Figure 29.

As Figure 30 shows, the moderate beam energy and resulting predominance of quasi-elastic reactions also allows precision measurement of θ_{23} and Δm^2_{23}.

[6] The neutrino spectra at this distance are identical to those at the far detector; the flux can therefore be extrapolated trivially as $1/r^2$.

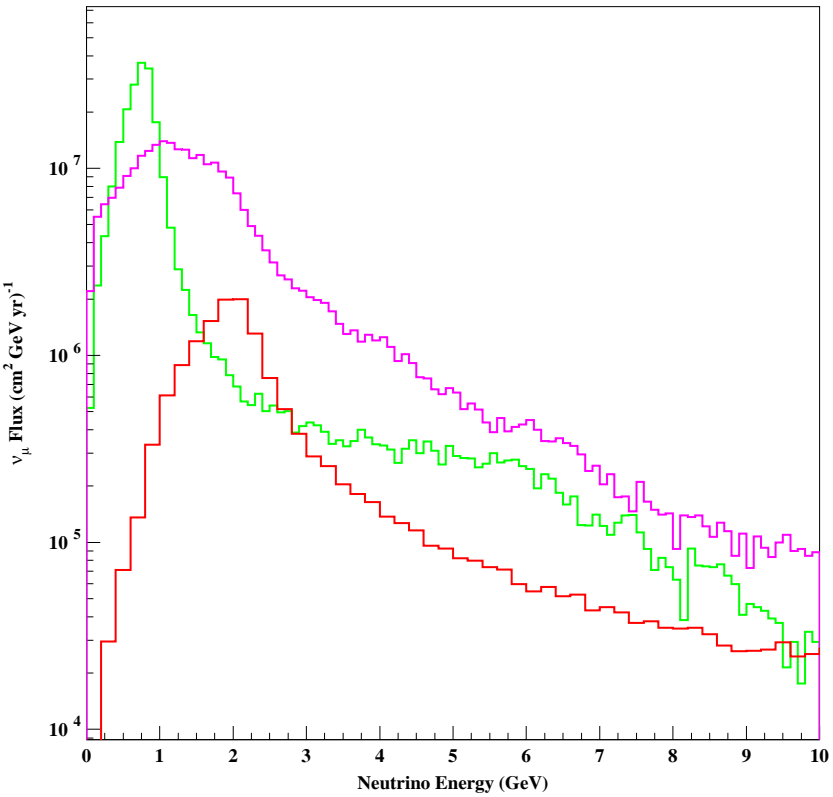

Figure 28: Comparison of the JHF wide-band (purple) and 2° off-axis (green) beams. The off-axis beam is narrowly peaked at an energy chosen to maximize the oscillation probability at 295 km for $\Delta m^2_{23} = 3 \times 10^{-3}\,\mathrm{eV}^2$, and the background-rich high-energy tail of the wide-band beam is suppressed. The higher-energy, NUMI (0.4 MW, Ph2LE) beam 10 km off-axis at 730 km is also shown (red).[38, 39]

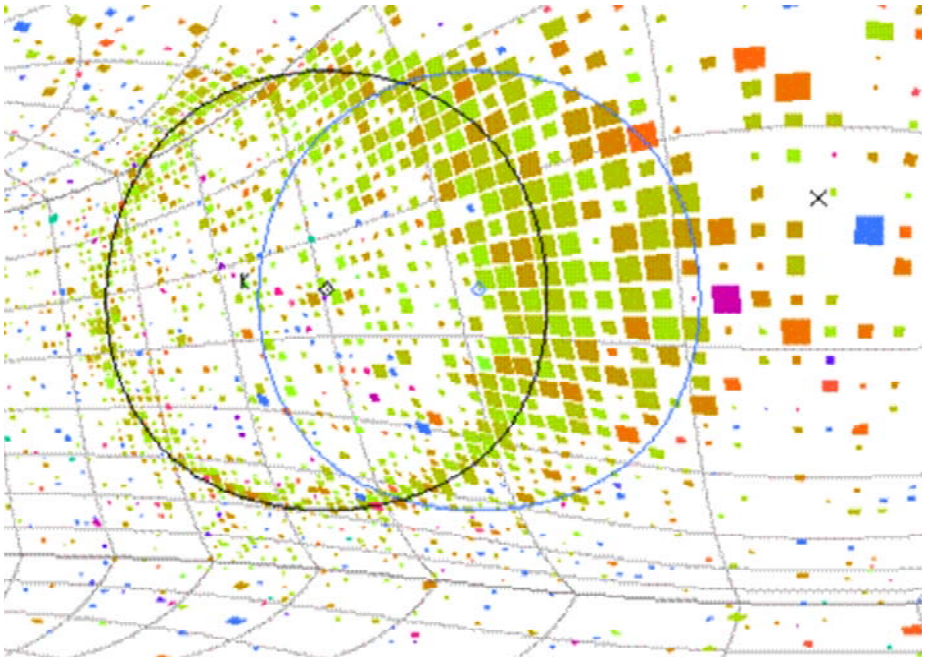

Figure 29: A real event from the K2K beam (which contains only 1% ν_e impurity) in Super–Kamiokande, demonstrating rejection of π^0 contamination in the future JHF-Kamioka project. Although only a single showering ring (the black circle at center) was evident in this event (making it appear to be ν_e-induced), a specialized likelihood fitter developed by American collaborators successfully identified another ring candidate (blue circle right of center) which, together with the primary ring, reconstructs to the π^0 mass and tags the event as a neutral current interaction. This event illustrates the importance of restoring the full inner detector photocathode coverage to any future ν_e appearance search, as well as proton decays involving π^0.

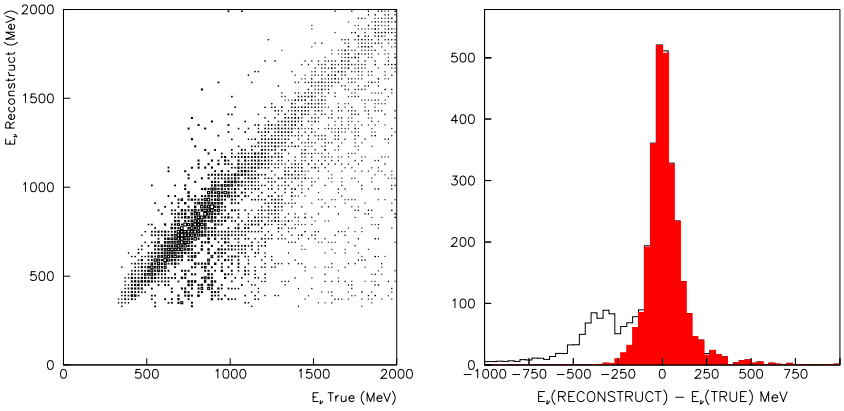

Figure 30: Neutrino energy reconstruction for the off-axis beam. Left: Reconstructed vs. true neutrino energy, showing a band of well-reconstructed quasi-elastic events along the diagonal, and feed-down of inelastic events. Right: Neutrino energy resolution, showing the contribution of quasi-elastic interactions (red) and the inelastic tail (unshaded). Charged-current quasi-elastic interactions allow the neutrino energy to be accurately determined using the measured lepton momentum and angle from the known beam direction. Inelastic events can subtracted when fitting the survival probability as a function L/E_ν^{recon} to extract Δm^2_{23}.[38]

Using only the detected lepton's momentum and angle, the incident neutrino energy can be inferred with sufficient precision to make the oscillatory pattern of ν_μ disappearance manifest when plotted vs. L/E_ν^{recon}. The position of the oscillation maximum permits precision measurement of Δm^2_{23}; comparison of the rate at $\langle E_{beam} \rangle$ compared to $E \gg \langle E_{beam} \rangle$ (using the unoscillated spectrum measured at the 1-2 km near detector as a reference) likewise provides a sensitive estimate of $\sin^2 2\theta_{23}$.

8.4 Phase I Sensitivity

It should be emphasized that efficiencies and backgrounds for the JHF-Kamioka project have been estimated using a neutrino interaction model validated by K2K near-detector data, a detector simulation tuned to agree precisely with the real experiment's performance over the first 5 years of operation, and reconstruction tools which are already in use. Hence, these projections of detector performance are in no sense optimistic "best guesses" typically found in preliminary studies but rather, conservative; with five years remaining to optimize JHF-specific analyses before the beam is available, improvements are certainly possible. This section describes the expected physics sensitivity of the Phase I experiment, as estimated by the Japanese JHF–Kamioka working group.[38]

Figure 31a shows the expected ν_e appearance signal and background in a five-year run (10^{21} protons on target), assuming $\sin^2 2\theta_{13}$ is near the upper-limit

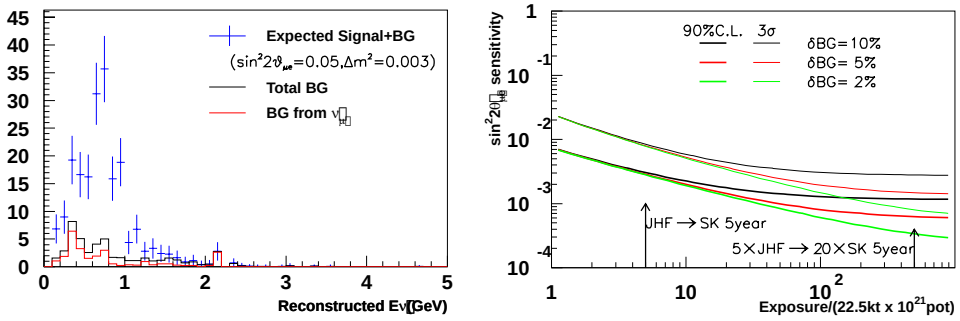

Figure 31: Left: Expected ν_e appearance signal (blue) and backgrounds (bottom histograms) in a five-year run, assuming the mixing angle $\sin^2 2\theta_{\mu e}$ (defined as $0.5\ \sin^2 2\theta_{13}$) is near the upper limit set by CHOOZ). Right: 90% confidence level (bottom curves) and 3σ (top) sensitivity to $\sin^2 2\theta_{\mu e}$ vs. exposure. A five-year run will improve the present CHOOZ limit by a factor of 20.[38]

set by CHOOZ. Figure 31b shows the projected 90% confidence level and 3σ sensitivities to the effective mixing angle $\sin^2 2\theta_{\mu e}$ ($\equiv 0.5 \sin^2 2\theta_{13}$) as a function of the exposure; for a five-year run the improvement is approximately a factor 20 over the present CHOOZ limit.

Turning to the ν_μ disappearance experiment, Figure 32 shows the clear oscillatory dependence of the ν_μ suppression on reconstructed neutrino energy after subtracting the background from inelastic events. Including reasonable systematic uncertainties, the survival probability can be fit to extract precisely ($\sim 1\%$) measured values of $\sin^2 2\theta_{23}$ and Δm^2_{23}, as demonstrated in Figure 33 for two values of $\sin^2 2\theta_{23}$.

Finally, the rate of neutral current interactions (tagged by single π^0) can be used to directly discriminate between the $\nu_\mu \to \nu_\tau$ and $\nu_\mu \to \nu_{sterile}$ oscillation hypotheses. Figure 34 shows the rate of identified single π^0 for both hypotheses, as a function of Δm^2_{23}. Since $\nu_\mu \to \nu_\tau$ oscillation does not reduce the rate of neutral current interactions, while full $\nu_\mu \to \nu_{sterile}$ mixing predicts more than a factor 2 suppression of the single π^0 rate, the measurement is sensitive to even small admixtures of $\nu_{sterile}$.

9 Budget

The incident that destroyed more than half the Super–Kamiokande detector's photomultiplier tubes is described in detail in our proposal. The budget presented here is for the reconstruction of the outer detector, a responsibility of the U.S. groups.

The KEK schedule calls for the neutrino beam to Super–Kamiokande to resume in January 2003, defining the date by which the detector must be operable. The commensurate reconstruction schedule requires that the PMT installation

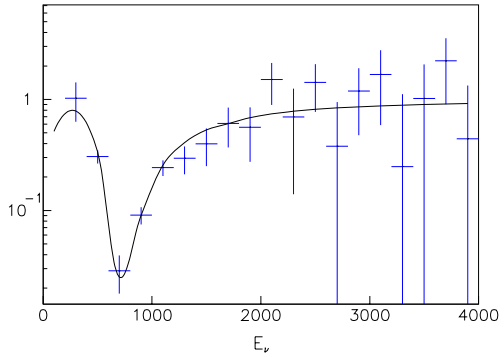

Figure 32: Probability of ν_μ survival as a function of reconstructed neutrino energy, after subtraction of inelastic background in a five-year run. The oscillatory pattern of the flux suppression is dramatically apparent.[38]

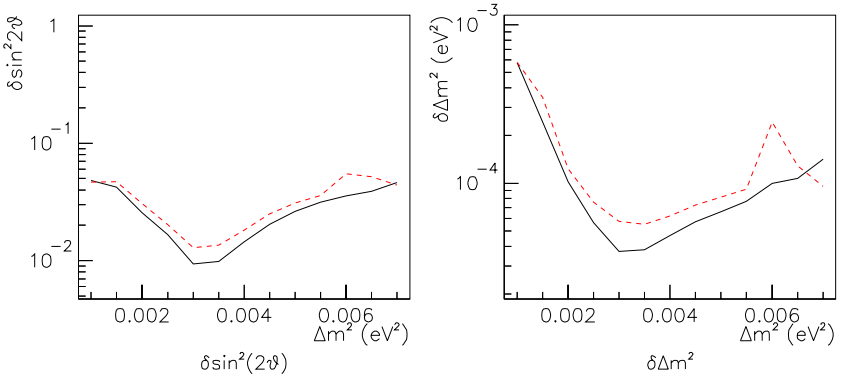

Figure 33: Measurement precision for $\sin^2 2\theta_{23}$ (left) and Δm^2_{23} (right) vs. Δm^2_{23}, for $\sin^2 2\theta_{23}$=1 (black curve) and 0.9 (red), for a five-year run. Both parameters can be determined with a precision of about 1%. Note that statistical and systematic errors are included in these estimates.[38]

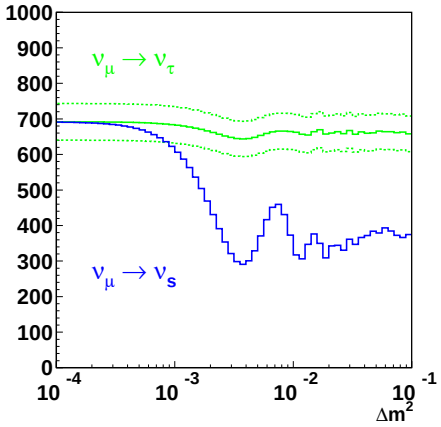

Figure 34: Comparison of single-π^0 event rates for $\nu_\mu \rightarrow \nu_\tau$ (green, showing a band with the uncertainty on the prediction) and $\nu_\mu \rightarrow \nu_{sterile}$ (blue) in a five-year run. The neutral current event rates allow the two hypotheses to be distinguished for all $\Delta m^2_{23} > 10^{-3}\,\mathrm{eV}^2$.[38]

commence in May with the main OD PMT replacement beginning in June 2002. This schedule places a restrictive timetable on placing orders for PMT's and other long-lead items.

Most budget items are for the PMT's and supporting equipment (cables, waveshifter plates, mounting plates and other hardware) plus other materials that will be installed permanently in the detector in the coming year. The remaining budget items support this reconstruction: i.e. safety equipment, supplies and materials, shipping, and personnel and travel costs.

References

[1] Y. Fukuda *et al.* [Super-Kamiokande Collaboration], Phys. Lett. B **433**, 9 (1998) [arXiv:hep-ex/9803006].

[2] K. S. Hirata *et al.* [KAMIOKANDE-II Collaboration], Phys. Lett. B **220**, 308 (1989).

[3] A. Suzuki, M. Mori, K. Kaneyuki, T. Tanimori, J. Takeuchi, H. Kyushima and Y. Ohashi, Nucl. Instrum. Meth. A **329**, 299 (1993).

[4] G. Altarelli and F. Feruglio, Phy. Lett. **B511** 257 (2001). hep-ph/0102301

[5] N. Arkani-Hamed and M. Schmaltz, Phy. Rev. **D61** 033005 (2000). hep-ph/9903417

[6] K. S. Babu and R. N. Mohapatra, Phys. Lett. B **518**, 269 (2001) [arXiv:hep-ph/0108089].

[7] S. J. Huber and Q. Shafi, Phys. Lett. B **512**, 365 (2001) [arXiv:hep-ph/0104293].

[8] J. Hufner and B. Z. Kopeliovich, Mod. Phys. Lett. A **13**, 2385 (1998) [arXiv:hep-ph/9807210].

[9] C. B. Dover, A. Gal and J. M. Richard, Phys. Rev. D **27**, 1090 (1983).

[10] M. Takita *et al.* [KAMIOKANDE Collaboration], Phys. Rev. D **34**, 902 (1986).

[11] M. Baldo-Ceolin *et al.*, Z. Phys. C **63**, 409 (1994).

[12] C. Berger *et al.* [Frejus Collaboration], Phys. Lett. B **240**, 237 (1990).

[13] J. Chung "Search for neutron oscillation and study of neutrino reaction rates using multiprong events in Soudan2", Tufts University *Ph.D.* thesis, September, 2001.

[14] T. Appelquist *et al.*, Phy. Rev. Lett. **87** 181802 (2001). hep-ph/0107056

[15] J.C. Pati, Proceedings of NNN99, Stony Brook, N.Y. (1999). hep-ph/0005095

[16] F. Wilczek, Proceedings of NNN99, Stony Brook, N.Y. (1999). hep-ph/0002045

[17] R. Dermisek, A. Mafi and S. Raby, Phy. Rev. **D63** 035001 (2001). hep-ph/0007213

[18] H. Georgi and S. Glashow, Phy. Rev. Lett. **32** 438 (1974).

[19] J. Ellis, J.S. Hagelin, and D.V. Nanopoulos, Phy. Lett. **B311** 1 (1998);
I. Antoniadis *et al.*, Phy. Lett. **B231** 65 (1989).

[20] D. Lee et al., Phy. Rev. **D51** 229 (1995).

[21] S. Dimopoulos and H. Georgi, Nucl. Phys. **B193** 150 (1981);
N. Sakai and T. Yanagida, Nucl. Phys. **B197** 83 (1982);
J. Hisano, H. Murayama, and T. Yanagida, Nucl. Phys. **B402** 46 (1993).

[22] P. Nath, A.H. Chamseddine, and R. Arnowitt, Phy. Rev. **D32** 2348 (1985);
P. Nath, and R. Arnowitt, Invited.

[23] G. Altarelli, F. Feruglio and I. Masina, JHEP 0011:040 (2000), hep-ph/0007254

[24] V. Lucas and S. Raby, Phy. Rev. **D55** 6986 (1997).
Q. Shafi and Z. Tavartkiladze, Phy. Lett. **B473** 272 (2000).

[25] K.S. Babu, J.C. Pati, and F. Wilczek, Nucl. Phy. **B566** 33 (2000);
ibid, Phy. Lett. **B423** (1998) 337;

[26] H. Ejiri, Phy. Rev. **C48** 1442 (1993).

[27] Y. Hayato *et al.*, Phy. Rev. Lett. **83** 1529 (1999). hep-ph/9904020

[28] Q. R. Ahmad *et al.* [SNO Collaboration], Phys. Rev. Lett. **87**, 071301 (2001) [arXiv:nucl-ex/0106015].

[29] T. Toshito [SuperKamiokande Collaboration], arXiv:hep-ex/0105023.

[30] Learned, J. G., et al, Proc. 25th Int. Cosmic Ray Conf, 1997.

[31] Stachyra, A., "Search for Astrophysical Point Sources of Neutrinos with Super-Kamiokande", University of Washington *Ph.D.* thesis, 2001.

[32] Y. Fukuda *et al.* [SuperKamiokande Collaboration], Phys. Lett. B **467**, 185 (1999) [arXiv:hep-ex/9908049].

[33] Y. Fukuda *et al.* [SuperKamiokande Collaboration], Phys. Rev. Lett. **82**, 2644 (1999) [arXiv:hep-ex/9812014].

[34] Y. Oyama *et al.* [KAMIOKANDE-II Collaboration], Phys. Rev. D **39**, 1481 (1989).

[35] Desai, S., "Search for Dark Matter WIMPs using Upward-Going Muons in Super–Kamiokande", Proc. 4th Int. Symp. on Sources and Detection of Dark Matter in the Universe", 2000.

[36] K. Langanke, P. Vogel and E. Kolbe, Phys. Rev. Lett. **76**, 2629 (1996) [arXiv:nucl-th/9511032].

[37] J. F. Beacom, R. N. Boyd and A. Mezzacappa, Phys. Rev. D **63**, 073011 (2001) [arXiv:astro-ph/0010398].

[38] Y. Itow *et al.*, arXiv:hep-ex/0106019.

[39] D. Harris and A. Para, private communication.